Lattice Boltzmann formulation for 8-wave magnetohydrodynamics

Paul J. Dellar

Mathematical Institute, University of Oxford, Radcliffe Observatory Quarter, Oxford OX2 6GG, UK

Magnetohydrodynamics couples the Navier–Stokes and Maxwell equations to describe flows in electrically conducting fluids. The divergence of the magnetic field must vanish, but numerical algorithms typically do not preserve this condition exactly. Artifacts can then arise in solutions, such as spurious forces parallel to the magnetic field. These artifacts can be alleviated by using extended sets of Maxwell's equations that include magnetic charges and currents, and hence are invariant under duality rotations that interchange the electric and magnetic fields. The 8-wave formulation supposes that the magnetic current arises from magnetic charges being advected by the fluid. The magnetohydrodynamic equations are then Galilean invariant even when the divergence of the magnetic field is non-zero. The evolution equation for the magnetic field resembles Jeffery's equation that describes the orientations of a suspension of axisymmetric particles. The ideal electric field is invariant under the extra terms proportional to the divergence of the magnetic field. This property leads to particularly simple lattice Boltzmann formulations for two of the three variants, with different treatments of the momentum equation, that are constructed and compared. The formulation that implements the Lorentz force directly, rather than via the Maxwell stress, proves more stable in numerical experiments.

Submitted 27 March 2024, revised 19 August 2024, accepted 30 September 2024 by the AIAA Journal.

I. Introduction

Magnetohydrodynamics (MHD) describes flows of electrically conducting fluids in magnetic fields by coupling the Navier–Stokes and Maxwell equations. The magnetic field $\mathbf{B}$ has the important property of having zero divergence. This can be treated as an initial condition that is preserved by the subsequent evolution. The divergence of Faraday's law, $\partial_t \mathbf{B} + \nabla\times\mathbf{E} = 0$, implies $\partial_t \nabla\cdot\mathbf{B} = 0$ for any electric field $\mathbf{E}$. However, $\nabla\cdot\mathbf{B} = 0$ is typically not preserved exactly in numerical simulations. A non-vanishing $\nabla\cdot\mathbf{B}$ can create artifacts because structural properties of the MHD equations fail to hold [1–3]. For example, the divergence of the Maxwell stress $\mathbf{BB} - \frac{1}{2}|\mathbf{B}|^2\mathbf{I}$ is no longer equal to the Lorentz force $(\nabla\times\mathbf{B})\times\mathbf{B}$, and no longer perpendicular to $\mathbf{B}$. More generally, when $\nabla\cdot\mathbf{B} \neq 0$, the magnetic force cannot be always perpendicular to the magnetic field in any numerical scheme that conserves momentum [2].

One can solve this problem by projecting the evolving magnetic field back onto a divergence-free vector field at every timestep [1, 4]. This projection is computationally expensive as it requires the solution of an elliptic equation. Instead, one can design special finite difference schemes that exactly preserve a particular discrete approximation to $\nabla\cdot\mathbf{B} = 0$ [2, 5, 6]. These are the ancestors of more recent mimetic discretisations [7]. They use discrete differential operators that satisfy an exact discrete analog of $\nabla\cdot(\nabla\times\mathbf{E}) \equiv 0$ for all vector fields $\mathbf{E}$. Alternatively, one can extend the MHD equations so that $\nabla\cdot\mathbf{B}$ evolves in time, and hence improve the structural properties of the MHD equations when $\nabla\cdot\mathbf{B}$ is not exactly zero. One can use this extra freedom to formulate a continuous-time analog of the discrete projection steps. This leads to the parabolic and hyperbolic divergence-cleaning formulations that introduce an additional scalar field into Faraday's law [8–12]. Powell's 8-wave formulation instead just advects $\nabla\cdot\mathbf{B}$ with the fluid velocity [13, 14]. This restores Galilean invariance to the MHD equations when $\nabla\cdot\mathbf{B} \neq 0$. The name "8-wave" comes from the additional contact discontinuity

that appears in the solution of the Riemann problem for compressible ideal MHD with this modification. These two approaches have been combined to evolve $\nabla\cdot\mathbf{B}$ using an extended telegraph equation that includes advection with the local fluid velocity [15, 16].

The lattice Boltzmann approach to simulating hydrodynamics uses a simplified Boltzmann equation with a discrete velocity space. The particle velocities are constrained to belong to a finite set, such that they propagate exactly from one lattice point to another over a fixed timestep [17–20]. Collisions between particles at lattice points are modeled by a linear relaxation towards a local equilibrium distribution that is a prescribed function of the local fluid density and velocity. The discrete velocity set and equilibrium distribution are constructed so that solutions that vary slowly compared with the timescale of collisions satisfy the isothermal Navier–Stokes equations, to within an error proportional to the cube of the Mach number. This error arises because the discrete velocity set is typically too small to capture the complete third moment of the continuous Maxwell–Boltzmann distribution, see Sec. III.B for details. The earlier discrete velocity models [21, 22] retain more qualitative properties of the real Boltzmann equation, such as binary collisions between pairs of particles, but their slowly varying solutions do not satisfy the Navier–Stokes equations, even for small Mach numbers. Models with larger numbers of discrete velocities merely approximate the Navier–Stokes equations more closely.

The lattice Boltzmann approach was soon extended to simulate two-dimensional MHD, using either a component of the magnetic vector potential [17], or a set of tensor-valued distribution functions [23, 24]. In both cases the fluid and the magnetic field were represented by one set of distribution functions. A later formulation adopted a more modular approach: a conventional hydrodynamic lattice Boltzmann formulation using scalar distribution functions coupled to a second set of vector-valued distribution functions for the magnetic field [25–27]. The two were coupled only through macroscopic variables, the fluid velocity and magnetic field, at lattice points. This formulation extended much more easily into three dimensions [28]. It has been used to perform what were then some of the largest simulations of three-dimensional MHD turbulence on an 1800^3 lattice [29], and to simulate liquid metal flows in bounded domains relevant to cooling systems for fusion reactors [28, 30, 31].

The vector lattice Boltzmann formulation of MHD includes parabolic divergence cleaning. The divergence of the magnetic field evolves according to $\partial_t\nabla\cdot\mathbf{B} = \eta\nabla^2\nabla\cdot\mathbf{B}$ for slowly varying solutions, where η is the resistivity. This has recently been extended to include hyperbolic divergence cleaning, either by adjusting the collision operator [32] or by explicitly introducing an additional scalar field [33]. A variant using a particular "magic" two-relaxation-time collision operator [34] has the mimetic property of exactly preserving a particular discrete approximation to $\nabla\cdot\mathbf{B} = 0$. The purpose of this paper is to implement Powell's 8-wave formulation in lattice Boltzmann MHD, exploiting its structural similarities with Jeffery's equation that describes the evolution of the orientation vectors in a suspension of axisymmetric particles [35–38]. This also leads naturally to a direct implementation of the Lorentz force in the momentum equation as an alternative to including the Maxwell stress in the momentum flux [28, 30].

II. Extended Maxwell equations for 8-wave magnetohydrodynamics

Maxwell's equations govern the evolution of the electric field $\mathbf{E}$ and magnetic field $\mathbf{B}$. They can be written in suitable electromagnetic units as [39, 40]

$$\nabla\cdot\mathbf{E} = \rho_e, \quad \nabla\cdot\mathbf{B} = 0, \quad \partial_t\mathbf{B} + \nabla\times\mathbf{E} = 0, \quad -(1/c^2)\partial_t\mathbf{E} + \nabla\times\mathbf{B} = \mathbf{J}_e, \tag{1}$$

for media without significant polarisation or magnetisation effects. Maxwell's equations support wave-like solutions that propagate with the speed of light c. There are sources of electric charge ρ_e and electric current $\mathbf{J}_e$ in the equations for $\nabla\cdot\mathbf{E}$ and $\partial_t\mathbf{E}$ respectively, but no corresponding sources in the equations for $\nabla\cdot\mathbf{B}$ and $\partial_t\mathbf{B}$.

The source-free Maxwell equations with $\rho_e = 0$ and $\mathbf{J}_e = 0$ are invariant under duality rotations by a constant angle

φ that transform $\mathbf{E}$ and $\mathbf{B}$ according to [40–42]

$$\mathbf{E} \mapsto \mathbf{E}\cos\varphi + c\mathbf{B}\sin\varphi, \quad \mathbf{B} \mapsto \mathbf{B}\cos\varphi - (1/c)\,\mathbf{E}\sin\varphi. \tag{2}$$

It is natural to consider an extended set of Maxwell equations with sources that remains invariant under duality rotations by introducing two extra sources: a magnetic charge ρ_m and a magnetic current $\mathbf{J}_m$ [40–42]

$$\nabla\cdot\mathbf{E} = \rho_e, \quad \nabla\cdot\mathbf{B} = \rho_m, \quad \partial_t\mathbf{B} + \nabla\times\mathbf{E} = -\mathbf{J}_m, \quad -(1/c^2)\partial_t\mathbf{E} + \nabla\times\mathbf{B} = \mathbf{J}_e. \tag{3}$$

These extended Maxwell equations reduce to the original Maxwell equations (1) when ρ_m and $\mathbf{J}_m$ both vanish.

To derive a closed set of equations we must relate the magnetic current vector $\mathbf{J}_m$ to the magnetic charge scalar ρ_m. Powell [13, 14] used the fluid velocity vector $\mathbf{u}$ to set $\mathbf{J}_m = \mathbf{u}\,\rho_m = \mathbf{u}\nabla\cdot\mathbf{B}$. This modification restores Galilean invariance to the MHD equations when $\nabla\cdot\mathbf{B} \neq 0$. The solution of the associated Riemann problem for compressible ideal MHD contains an additional "8th wave" contact discontinuity that advects $\nabla\cdot\mathbf{B}$ with the fluid velocity normal to the initial discontinuity.

However, a lattice Boltzmann formulation naturally targets resistive MHD instead of ideal MHD. It is then more natural to take

$$\mathbf{J}_m = \mathbf{u}\rho_m - \eta\nabla\rho_m, \tag{4}$$

where η is a constant resistivity, just as the electric field is given by Ohm's law

$$\mathbf{E} = -\mathbf{u}\times\mathbf{B} + \eta\nabla\times\mathbf{B}. \tag{5}$$

The induction equation for evolving $\mathbf{B}$ with these two fields $\mathbf{E}$ and $\mathbf{J}_m$ then becomes

$$\begin{aligned}\partial_t\mathbf{B} &= \nabla\times(\mathbf{u}\times\mathbf{B} - \eta\nabla\times\mathbf{B}) - \mathbf{u}\nabla\cdot\mathbf{B} + \eta\nabla\nabla\cdot\mathbf{B},\\ &= \nabla\times(\mathbf{u}\times\mathbf{B}) - \mathbf{u}\nabla\cdot\mathbf{B} + \eta\nabla^2\mathbf{B}.\end{aligned} \tag{6}$$

Taking the divergence of this induction equation gives

$$\partial_t(\nabla\cdot\mathbf{B}) + \nabla\cdot(\mathbf{u}\nabla\cdot\mathbf{B}) = \eta\nabla^2(\nabla\cdot\mathbf{B}). \tag{7}$$

The magnetic charge density advects with the fluid velocity $\mathbf{u}$, and diffuses with the resistivity η. The right-hand side was already present in the lattice Boltzmann MHD formulation, which implements the equivalent of $\mathbf{J}_m = -\eta\nabla(\nabla\cdot\mathbf{B})$, and thus supports parabolic divergence cleaning [8, 10, 25, 32]. The extra $\mathbf{u}\nabla\cdot\mathbf{B}$ term on the left-hand side implements Powell's 8-wave formulation [13, 14].

An equation very like (6) arises in another context to describe dilute suspensions of axisymmetric particles in viscous fluids. The field $\mathbf{p}$ of orientation vectors for the particles evolves according to Jeffery's equation [35–37]

$$\partial_t\mathbf{p} + \mathbf{u}\cdot\nabla\mathbf{p} = \mathbf{p}\cdot\nabla\mathbf{u} + (\beta - 1)\,\mathbf{E}\cdot\mathbf{p} - \beta\,\mathbf{p}\,\mathbf{p}\cdot\mathbf{E}\cdot\mathbf{p}, \tag{8}$$

where $\mathbf{E} = (\nabla\mathbf{u}) + (\nabla\mathbf{u})^{\mathrm{T}}$ is the symmetric strain rate tensor. The dependence on the particle shape is expressed by the Bretherton parameter β. In particular, $\beta \to 1$ as the particles become more elongated. The nonlinear term involving $\mathbf{p}\cdot\mathbf{E}\cdot\mathbf{p}$ preserves the normalisation $|\mathbf{p}| = 1$. The vector field $\mathbf{P} = \rho\mathbf{p}$ in a compressible fluid thus evolves according to [38]

$$\partial_t\mathbf{P} = \nabla\times(\mathbf{u}\times\mathbf{P}) - \mathbf{u}\,\nabla\cdot\mathbf{P} + (\beta - 1)\,\mathbf{E}\cdot\mathbf{P} - (\beta/\rho^2)\,\mathbf{P}\,\mathbf{P}\cdot\mathbf{E}\cdot\mathbf{P}. \tag{9}$$

The first two terms on the right-hand side match the corresponding terms in (6) above. For very elongated particles with $\beta = 1$, the only differences are the extra normalisation term to preserve $|\mathbf{p}| = 1$, and the lack of diffusion.

A. Symmetric hyperbolic structure

The discussion above only involved the induction equation for evolving the magnetic field. The $\nabla\cdot\mathbf{B} = 0$ condition is an involution of the MHD equations [3, 43, 44]. This condition is preserved by the subsequent evolution if it holds initially. We can therefore add terms proportional to $\nabla\cdot\mathbf{B}$ to the momentum equation as well. Powell [13, 14] used this freedom to add an extra source term in the momentum equation. The complete system, for compressible ideal MHD with constant temperature and no independent energy equation, is

$$\frac{\partial}{\partial t}\begin{pmatrix}\rho\\ \rho\mathbf{u}\\ \mathbf{B}\end{pmatrix} + \nabla\cdot\begin{pmatrix}\rho\mathbf{u}\\ \rho\mathbf{u}\mathbf{u} + \rho\theta\mathbf{I} + \frac{1}{2}|\mathbf{B}|^2\mathbf{I} - \mathbf{B}\mathbf{B}\\ \mathbf{u}\mathbf{B} - \mathbf{B}\mathbf{u}\end{pmatrix} = -\nabla\cdot\mathbf{B}\begin{pmatrix}0\\ \mathbf{B}\\ \mathbf{u}\end{pmatrix}. \tag{10}$$

The gas pressure is $p = \rho\theta$, where θ is the temperature in the so-called energy units that absorb the gas constant into θ. The Newtonian sound speed for small isothermal density perturbations is $\sqrt{\theta}$ in these units. We use a dyadic notation in which $\mathbf{u}\mathbf{u}$ denotes the rank-2 tensor with components $u_\alpha u_\beta$, and $\mathbf{u}\mathbf{B} - \mathbf{B}\mathbf{u}$ denotes the rank-2 tensor with components $u_\alpha B_\beta - B_\alpha u_\beta$. We use Greek indices for vector and tensor components, reserving Roman indices for labelling discrete velocities.

The system (10) coincides with the isentropic version of the system constructed by Godunov [45] to transform the ideal MHD equations into a hyperbolic system that is symmetrisable in the sense of Friedrichs, and hence benefits from local well-posedness results for systems of this form [46, 47]. Godunov's formulation included a separate energy equation, and used the gas-dynamic entropy as the symmetrising variable [45]. The isentropic system (10) is more similar to the symmetrisable form of the shallow water MHD equations [48].

The momentum equation in (10) can be rewritten as

$$\partial_t(\rho\mathbf{u}) + \nabla\cdot(\rho\mathbf{u}\mathbf{u} + \rho\theta\mathbf{I}) = (\nabla\times\mathbf{B})\times\mathbf{B} \tag{11}$$

even when $\nabla\cdot\mathbf{B} \neq 0$. We have the standard definition of the Lorentz force on the right-hand side, so the force exerted by the magnetic field is always perpendicular to $\mathbf{B}$. This avoids the artifacts due to magnetic charges experiencing forces parallel to the magnetic field identified in [1]. However, this evolution equation for linear momentum cannot be written solely in terms of the divergence of a momentum flux when $\nabla\cdot\mathbf{B} \neq 0$.

B. Hamiltonian structure

The ideal MHD equations have other structural properties that one might want to preserve when $\nabla\cdot\mathbf{B} \neq 0$. In particular, the ideal MHD equations can be expressed as a non-canonical Hamiltonian field theory [49, 50]. This formalism abstracts the geometrical properties of Hamiltonian particle mechanics to accommodate ideal continuum mechanics using Eulerian variables. The evolution of any functional $\mathcal{F}$ of the field variables ρ, $\mathbf{u}$, $\mathbf{B}$ is given by

$$\dot{\mathcal{F}} = \{\mathcal{F}, \mathcal{H}\}, \tag{12}$$

where $\mathcal{H}$ is the Hamiltonian functional. The Poisson bracket $\{\cdot,\cdot\}$ is an antisymmetric bilinear form that satisfies the Jacobi identity $\{\{\mathcal{F},\mathcal{G}\},\mathcal{K}\} + \{\{\mathcal{G},\mathcal{K}\},\mathcal{F}\} + \{\{\mathcal{K},\mathcal{F}\},\mathcal{G}\} = 0$ for all functionals $\mathcal{F}$, $\mathcal{G}$, and $\mathcal{K}$. The canonical Poisson bracket from Hamiltonian particle mechanics has all these properties.

The Poisson bracket that yields isothermal compressible magnetohydrodynamics is [49, 51]

$$\begin{aligned}\{\mathcal{F},\mathcal{G}\} = \int m_\alpha\left(\frac{\delta\mathcal{G}}{\delta m_\beta}\partial_\beta\frac{\delta\mathcal{F}}{\delta m_\alpha} - \frac{\delta\mathcal{F}}{\delta m_\beta}\partial_\beta\frac{\delta\mathcal{G}}{\delta m_\alpha}\right) + \rho\left(\frac{\delta\mathcal{G}}{\delta m_\alpha}\partial_\alpha\frac{\delta\mathcal{F}}{\delta\rho} - \frac{\delta\mathcal{F}}{\delta m_\alpha}\partial_\alpha\frac{\delta\mathcal{G}}{\delta\rho}\right)\\ + B_\alpha\left(\frac{\delta\mathcal{G}}{\delta m_\beta}\partial_\beta\frac{\delta\mathcal{F}}{\delta B_\alpha} - \frac{\delta\mathcal{F}}{\delta m_\beta}\partial_\beta\frac{\delta\mathcal{G}}{\delta B_\alpha}\right) - B_\beta\left(\frac{\delta\mathcal{G}}{\delta B_\alpha}\partial_\beta\frac{\delta\mathcal{F}}{\delta m_\alpha} - \frac{\delta\mathcal{F}}{\delta B_\alpha}\partial_\beta\frac{\delta\mathcal{G}}{\delta m_\alpha}\right)\mathrm{d}V,\end{aligned} \tag{13}$$

where $\mathbf{m} = \rho\mathbf{u}$ is the momentum density. This Poisson bracket has the special property that each term is linear in one of the field variables ρ, $\mathbf{m}$, $\mathbf{B}$, so the Jacobi identity can be established relatively easily [49, 50]. The Hamiltonian functional is the integral of the kinetic, internal, and magnetic energy densities,

$$\mathcal{H} = \int \frac{1}{2}\rho|\mathbf{u}|^2 + \mathcal{U}(\rho) + \frac{1}{2}|\mathbf{B}|^2 \mathrm{d}V. \tag{14}$$

The internal energy density is $\mathcal{U}(\rho) = \theta\rho\log(\rho/\rho_0)$ for an isothermal equation of state with $p = \rho\theta$. The constant ρ_0 is needed for dimensional correctness but does not appear in the evolution equations. Changing ρ_0 changes $\mathcal{H}$ by a multiple of the total mass, which is separately conserved.

The momentum equation obtained from (12) and (13) can be written in divergence form as

$$\partial_t m_\beta + \partial_\alpha \Pi_{\alpha\beta} = 0, \tag{15}$$

using the momentum flux tensor [52]

$$\Pi_{\alpha\beta} = m_\beta \frac{\delta\mathcal{H}}{\delta m_\alpha} - B_\alpha \frac{\delta\mathcal{H}}{\delta B_\beta} + \delta_{\alpha\beta}\left(m_\gamma \frac{\delta\mathcal{H}}{\delta m_\gamma} + \rho\frac{\delta\mathcal{H}}{\delta\rho} + B_\gamma \frac{\delta\mathcal{H}}{\delta B_\gamma} - H\right). \tag{16}$$

This holds for any Hamiltonian functional $\mathcal{H} = \int H\,\mathrm{d}V$ whose integrand H is an algebraic function of ρ, $\mathbf{m}$, $\mathbf{B}$. It follows from the invariance of the Hamiltonian and Poisson bracket under spatial translations via Noether's theorem. Conversely, the evolution equation for $\mathbf{B}$ obtained fom (12) and (13) contains the curl of the electric field vector, and a second term proportional to $\nabla\cdot\mathbf{B}$ that cannot be written as a divergence of a flux,

$$\partial_t \mathbf{B} + \nabla\times\left(-\frac{\delta\mathcal{H}}{\delta\mathbf{m}}\times\mathbf{B}\right) + \frac{\delta\mathcal{H}}{\delta\mathbf{m}}\nabla\cdot\mathbf{B} = 0. \tag{17}$$

This matches the ideal ($\eta = 0$) version of the induction equation (6) above, as $\delta\mathcal{H}/\delta\mathbf{m} = \mathbf{u}$ for the Hamiltonian in (14).

Another argument [53] for seeking a momentum evolution equation in the divergence form (15) when $\nabla\cdot\mathbf{B} \neq 0$ notes that the full electromagnetic Maxwell stress [39, 40]

$$\mathbf{BB} + \frac{1}{c^2}\mathbf{EE} - \frac{1}{2}\left(|\mathbf{B}|^2 + \frac{1}{c^2}|\mathbf{E}|^2\right)\mathbf{I} \tag{18}$$

is invariant under duality rotations. The force exerted by an electric field is the divergence of the electric part of the Maxwell stress even when $\nabla\cdot\mathbf{E} \neq 0$. One might therefore expect the force exerted by a magnetic field to be the divergence of the magnetic part of the Maxwell stress even when $\nabla\cdot\mathbf{B} \neq 0$.

III. Lattice Boltzmann hydrodynamics

The Boltzmann equation describes the evolution of the distribution $f(\mathbf{x}, \boldsymbol{\xi}, t)$ of particles at position $\mathbf{x}$ at time t moving with velocity $\boldsymbol{\xi}$ in a dilute monatomic gas [54]

$$\partial_t f + \boldsymbol{\xi}\cdot\nabla f + \mathbf{a}\cdot\nabla_{\boldsymbol{\xi}} f = C[f, f]. \tag{19}$$

The left-hand side includes an external acceleration $\mathbf{a}$ exerted on the particles, for instance by gravity. The right-hand side denotes Boltzmann's binary collision operator. Taking moments of (19) yields the hydrodynamic equations

$$\partial_t\rho + \nabla\cdot(\rho\mathbf{u}) = 0, \quad \partial_t(\rho\mathbf{u}) + \nabla\cdot\boldsymbol{\Pi} = \mathbf{F}, \tag{20a}$$

$$\partial_t\boldsymbol{\Pi} + \nabla\cdot\mathbf{Q} = -\frac{1}{\tau}\left(\boldsymbol{\Pi} - \boldsymbol{\Pi}^{(0)}\right) + \mathbf{Fu} + \mathbf{uF}, \tag{20b}$$

where $\mathbf{F} = \rho\mathbf{a}$ is the force density due to the external acceleration. We write $\mathbf{F}$ on the right-hand sides because the contributions from $\mathbf{a}\cdot\nabla_{\boldsymbol{\xi}} f$ become algebraic terms after integration in $\boldsymbol{\xi}$. The quantities appearing in (20a,b) are the fluid density ρ and velocity $\mathbf{u}$, the momentum flux $\boldsymbol{\Pi}$, and the third moment $\mathbf{Q}$, defined in terms of f by

$$\rho = \int f\mathrm{d}\boldsymbol{\xi}, \quad \rho\mathbf{u} = \int \boldsymbol{\xi} f\mathrm{d}\boldsymbol{\xi}, \quad \boldsymbol{\Pi} = \int \boldsymbol{\xi}\boldsymbol{\xi} f\mathrm{d}\boldsymbol{\xi}, \quad \mathbf{Q} = \int \boldsymbol{\xi}\boldsymbol{\xi}\boldsymbol{\xi} f\mathrm{d}\boldsymbol{\xi}. \tag{21}$$

The collision operator does not contribute to the mass and momentum conservation equations in (20a) as binary collisions between pairs of particles conserve particle number and momentum. However, collisions have the effect of relaxing the momentum flux $\mathbf{\Pi}$ towards its equilibrium value $\mathbf{\Pi}^{(0)} = \rho\theta\mathbf{I} + \rho\mathbf{u}\mathbf{u}$ over a timescale τ. This is an exact property of the linearised Boltzmann collision operator for Maxwell molecules, hypothetical particles that interact via an inverse fifth-power repulsion, and otherwise a good approximation.

A. Recovering hydrodynamics

For solutions that evolve very slowly on timescales T much longer than the collision time τ, we can set $\mathbf{\Pi}$ equal to $\mathbf{\Pi}^{(0)}$ at leading order. The temperature θ is commonly taken to be constant when constructing a discrete kinetic theory for nearly incompressible flows for which the Mach number $\mathrm{Ma} = |\mathbf{u}|/\sqrt{\theta}$ is small. The system (21) then describes the compressible Euler equations with constant temperature θ. To proceed further, we pose a multiple-scales expansion of $\mathbf{\Pi}$, $\mathbf{Q}$ and the time derivative ∂_t as

$$\mathbf{\Pi} = \mathbf{\Pi}^{(1)} + \mathbf{\Pi}^{(1)} + \cdots, \quad \mathbf{Q} = \mathbf{Q}^{(0)} + \mathbf{Q}^{(1)} + \cdots, \quad \partial_t = \partial_{t_0} + \partial_{t_1} + \cdots, \tag{22}$$

while leaving ρ and $\mathbf{u}$ unexpanded. These expansions should in principle be written explicitly using powers of the dimensionless small parameter $\epsilon = \tau/T$, the Knudsen number, but it is common to absorb the powers of τ into the terms of the series, as in the expression (26) for $\mathbf{\Pi}^{(1)}$ below.

The leading-order approximation to the evolution equation (20b) for $\mathbf{\Pi}$ is then

$$\partial_{t_0}\mathbf{\Pi}^{(0)} + \nabla\cdot\mathbf{Q}^{(0)} = -\frac{1}{\tau}\mathbf{\Pi}^{(1)} + \mathbf{F}\mathbf{u} + \mathbf{u}\mathbf{F}. \tag{23}$$

The multiple-scales expansion of the time derivative allows us to evaluate

$$\begin{aligned}
\partial_{t_0}\mathbf{\Pi}^{(0)} &= \partial_{t_0}(\rho\theta\mathbf{I} + \rho\mathbf{u}\mathbf{u}),\\
&= \mathbf{u}\partial_{t_0}(\rho\mathbf{u}) + \partial_{t_0}(\rho\mathbf{u})\mathbf{u} + (\theta\mathbf{I} - \mathbf{u}\mathbf{u})\partial_{t_0}\rho,\\
&= \mathbf{u}\mathbf{F} - \mathbf{u}(\nabla\cdot\mathbf{\Pi}^{(0)}) + \mathbf{F}\mathbf{u} - (\nabla\cdot\mathbf{\Pi}^{(0)})\mathbf{u} - (\theta\mathbf{I} - \mathbf{u}\mathbf{u})\nabla\cdot(\rho\mathbf{u}),
\end{aligned} \tag{24}$$

using the Euler equations $\partial_{t_0}\rho + \nabla\cdot(\rho\mathbf{u}) = 0$ and $\partial_{t_0}(\rho\mathbf{u}) + \nabla\cdot\mathbf{\Pi}^{(0)} = \mathbf{F}$. The $\mathbf{F}\mathbf{u} + \mathbf{u}\mathbf{F}$ contribution from $\mathbf{a}\cdot\nabla_{\boldsymbol{\xi}} f$ in (23) exactly cancels with the contribution from $\partial_{t_0}\mathbf{\Pi}^{(0)}$ in (24). The third moment $\mathbf{Q}^{(0)}$ of the Maxwell–Boltzmann distribution has components

$$Q^{(0)}_{\alpha\beta\gamma} = \rho u_\alpha u_\beta u_\gamma + \rho\theta\left(u_\alpha\delta_{\beta\gamma} + u_\beta\delta_{\gamma\alpha} + u_\gamma\delta_{\alpha\beta}\right). \tag{25}$$

We thus obtain the Newtonian viscous stress

$$\mathbf{\Pi}^{(1)} = -\tau\rho\theta\left((\nabla\mathbf{u}) + (\nabla\mathbf{u})^{\mathrm{T}}\right) \tag{26}$$

for a fluid with dynamic viscosity $\mu = \tau\rho\theta$. The viscous stress is unaffected by the external acceleration $\mathbf{a}$. Comparing this expression with $\mathbf{\Pi}^{(0)} = \rho\theta\mathbf{I} + \rho\mathbf{u}\mathbf{u}$ shows that $\mathbf{\Pi}^{(1)} = O(\epsilon\mathbf{\Pi}^{(0)})$ with $\epsilon = \tau/T$, and determines the hydrodynamic timescale T from the fluid velocity gradient via $||\nabla\mathbf{u}|| = O(1/T)$.

B. Discrete kinetic theory

We formulate a discrete kinetic theory by restricting the particle velocity $\boldsymbol{\xi}$ to a discrete set of N velocities $\boldsymbol{\xi}_0, \ldots, \boldsymbol{\xi}_{N-1}$ and replacing $f(\mathbf{x}, \boldsymbol{\xi}, t)$ by a discrete set of functions $f_i(\mathbf{x}, t)$. The hydrodynamic variables are now given by the discrete moments

$$\rho = \sum_{i=0}^{N-1} f_i, \quad \rho\mathbf{u} = \sum_{i=0}^{N-1} \boldsymbol{\xi}_i f_i, \quad \mathbf{\Pi} = \sum_{i=0}^{N-1} \boldsymbol{\xi}_i\boldsymbol{\xi}_i f_i, \quad \mathbf{Q} = \sum_{i=0}^{N-1} \boldsymbol{\xi}_i\boldsymbol{\xi}_i\boldsymbol{\xi}_i f_i. \tag{27}$$

The f_i are postulated to evolve according to a discrete velocity Boltzmann equation,

$$\partial_t f_i + \boldsymbol{\xi}_i \cdot \nabla f_i = -\sum_{j=0}^{N-1} \Omega_{ij} \left(f_j - f_j^{(0)} \right) + R_i. \tag{28}$$

The first term on the right-hand side represents a general linear collision operator that relaxes the f_i towards some equilibrium values $f_j^{(0)}$ with a relaxation matrix $\boldsymbol{\Omega}$. The matrix elements Ω_{ij} are usually constants, but we will later take them to be functions of the macroscopic variables $\mathbf{u}$ and $\mathbf{B}$. The $f_j^{(0)}$ are prescribed functions of the fluid density and velocity. They are the discrete analog of the Maxwell–Boltzmann distribution.

A common choice is [55]

$$f_i^{(0)} = w_i \left(\rho + \frac{1}{\theta} \boldsymbol{\xi}_i \cdot (\rho \mathbf{u}) + \frac{1}{2\theta^2} (\boldsymbol{\xi}_i \boldsymbol{\xi}_i - \theta \mathbf{I}) : (\boldsymbol{\Pi}^{(0)} - \rho\theta \mathbf{I}) \right), \tag{29}$$

with $\theta = 1/3$ in so-called lattice units in which the components of the discrete velocities $\boldsymbol{\xi}_i$ take the values $-1, 0, 1$. The expressions 1, $\boldsymbol{\xi}_i$ and $\boldsymbol{\xi}_i \boldsymbol{\xi}_i - \theta \mathbf{I}$ are three of Grad's tensor Hermite polynomials, and the weights w_i arise from a Gauss–Hermite quadrature [56]. These weights are $w_0 = 4/9$, $w_{1,2,3,4} = 1/9$ and $w_{5,6,7,8} = 1/36$ for the nine discrete velocities $\boldsymbol{\xi}_i$ shown in Fig. 1.

The second term R_i on the right-hand side of (28) approximates the $\mathbf{a} \cdot \nabla_{\boldsymbol{\xi}} f$ term in the Boltzmann equation (19). The same reasoning that leads to (29) as an expansion in tensor Hermite polynomials gives [57]

$$R_i = w_i \left(\frac{1}{\theta} \boldsymbol{\xi}_i \cdot \mathbf{F} + \frac{1}{2\theta^2} (\boldsymbol{\xi}_i \boldsymbol{\xi}_i - \theta \mathbf{I}) : (\mathbf{F}\mathbf{u} + \mathbf{u}\mathbf{F}) \right). \tag{30}$$

For suitable choices of the matrix $\boldsymbol{\Omega}$, we can derive the same evolution equation for $\boldsymbol{\Pi}$ that appeared in (20b). This requires

$$\sum_{i=0}^{N-1} \boldsymbol{\xi}_i \boldsymbol{\xi}_i \left(-\sum_{j=0}^{N-1} \Omega_{ij} \left(f_j - f_j^{(0)} \right) \right) = -\frac{1}{\tau} \left(\boldsymbol{\Pi} - \boldsymbol{\Pi}^{(0)} \right), \tag{31}$$

for some relaxation time τ, so $\boldsymbol{\Pi}$ is an eigenfunction of the collision operator on the right-hand side of (28) with eigenvalue $-1/\tau$. We can then apply the exact same steps from Sec. III.A to the discrete Boltzmann equation (28) and recover the same compressible Navier–Stokes equations with a body force $\mathbf{F}$. The only difference is that the equilibrium third moment $\mathbf{Q}^{(0)}$ calculated from (29) is missing the $\rho\mathbf{uuu}$ term that is present in the corresponding moment (25) of the Maxwell–Boltzmann distribution. The viscous stress thus contains an error term proportional to $|\mathbf{u}|^3$ [58]. This term is $O(\mathrm{Ma}^2)$ smaller than the Newtonian viscous stress, and hence negligible for nearly incompressible flows.

C. Discretisation by Strang splitting

We now discretise the discrete Boltzmann equation (28) in space and time to construct a lattice Boltzmann equation for hydrodynamics. We do this using Strang splitting to treat the left and right-hand sides of (28) separately [59, 60]. The left-hand side alone, $\partial_t f_i + \boldsymbol{\xi}_i \cdot \nabla f_i = 0$, describes the advection of each f_i along a straight characteristic with constant velocity $\boldsymbol{\xi}_i$. The exact solution over a timestep Δt is given by the shift operator S defined by

$$(\mathsf{S} f_i)(\mathbf{x}, t) = f_i(\mathbf{x} - \boldsymbol{\xi}_i \Delta t, t). \tag{32}$$

The remaining part of the evolution comprises a system of ordinary differential equations in time,

$$\partial_t f_i = -\sum_{j=0}^{N-1} \Omega_{ij} \left(f_j - f_j^{(0)} \right) + R_i. \tag{33}$$

These can be discretised using the Crank–Nicolson method [61] with second-order accuracy in Δt to define a collision operator C. Writing $\mathbf{f} = (f_0, \ldots, f_{N-1})^{\mathrm{T}}$ as a column vector for ease of notation, the Crank–Nicolson [61] discretisation

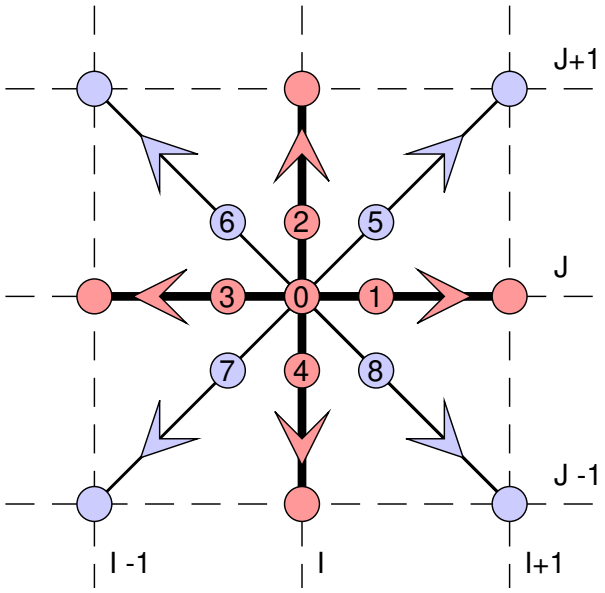

Fig. 1 The nine discrete velocities $\boldsymbol{\xi}_0, \ldots, \boldsymbol{\xi}_8$ that form the D2Q9 lattice used for the f_i, and the five discrete velocities $\boldsymbol{\xi}_0, \ldots, \boldsymbol{\xi}_4$ shown in red with thicker lines that form the D2Q5 lattice used for the $\mathbf{g}_i$.

of (33) is

$$\mathbf{f}' - \mathbf{f} = -\tfrac{1}{2}\Delta t\boldsymbol{\Omega}\left(\mathbf{f} + \mathbf{f}' - \mathbf{f}^{(0)} - \mathbf{f}'^{(0)}\right) + \tfrac{1}{2}\Delta t\,(\mathbf{R} + \mathbf{R}'), \tag{34}$$

where a prime denotes a post-collisional quantity evaluated at time $t + \Delta t$. An unprimed quantity is evaluated at time t. The post-collisional equilibrium distributions in the vector $\mathbf{f}'^{(0)}$ are known functions of ρ and $\mathbf{u}$. In the simplest case with no body force, $\mathbf{f}'^{(0)} = \mathbf{f}^{(0)}$ and $\mathbf{R}$ vanishes, so we can easily solve for

$$\mathbf{f}' = \mathbf{f} - \left(\mathbf{I} + \tfrac{1}{2}\Delta t\boldsymbol{\Omega}\right)^{-1}\Delta t\boldsymbol{\Omega}\left(\mathbf{f} - \mathbf{f}^{(0)}\right). \tag{35}$$

This defines the collision operator C. The matrix $\boldsymbol{\Omega} = (1/\tau)\mathbf{I}$ is a scalar multiple of the identity matrix for the Bhatnagar–Gross–Krook [62] collision operator with a single relaxation time τ, so we can solve separately for each f_i,

$$f_i' = f_i - \frac{\Delta t}{\tau + \Delta t/2}\left(f_i - f_i^{(0)}\right) \tag{36}$$

for $i = 0, \ldots, N-1$. This resembles a forward Euler discretisation of the ordinary differential equations, except τ has been replaced by $\tau + \Delta t/2$ in the denominator. The overall numerical scheme simulates a fluid with viscosity $\mu = \tau\rho\theta$ but the discrete relaxation time is $\tau + \Delta t/2$ rather than τ. This so-called Hénon correction [63] of the relaxation time raises the accuracy from first order to second order in Δt. The case with a body force is best dealt with using a basis of moments, as in the next section, but proceeding from (34) by expressing $\mathbf{f}'^{(0)}$ in terms of ρ, $\mathbf{u}$ and the body force leads to exactly the same result [64].

Using Strang splitting [59] we can approximate the solution of (28) by*

$$f_i(\mathbf{x}, t + \Delta t) = \mathsf{S}^{1/2}\,\mathsf{C}\,\mathsf{S}^{1/2}\,f_i(\mathbf{x}, t), \tag{37}$$

where $\mathsf{S}^{1/2}$ denotes the action of the streaming operator for a half timestep,

$$(\mathsf{S}^{1/2}f_i)(\mathbf{x}, t) = f_i(\mathbf{x} - \tfrac{1}{2}\boldsymbol{\xi}_i\Delta t, t). \tag{38}$$

This symmetric composition of $\mathsf{S}^{1/2}\mathsf{C}\mathsf{S}^{1/2}$ in (37) gives second-order accuracy in Δt by eliminating the leading-order splitting error [59]. Applying this formula for n timesteps gives

$$f_i(\mathbf{x}, t + n\Delta t) = \mathsf{S}^{1/2}\,\mathsf{C}\,\mathsf{S}^{1/2}\,\mathsf{S}^{1/2}\,\mathsf{C}\,\mathsf{S}^{1/2}\,\ldots\,\mathsf{S}^{1/2}\,\mathsf{C}\,\mathsf{S}^{1/2}\,f_i(\mathbf{x}, t). \tag{39}$$

*Martin Geier, 2024, personal communication

Using $\mathsf{S}^{1/2}\,\mathsf{S}^{1/2} = \mathsf{S}$ to combine the intermediate stages gives

$$f_i(\mathbf{x}, t + n\Delta t) = \mathsf{S}^{-1/2}\,\mathsf{S}\,\mathsf{C}\,\mathsf{S}\,\mathsf{C}\,\mathsf{S}\,\ldots\,\mathsf{C}\,\mathsf{S}\,\mathsf{C}\,\mathsf{S}^{1/2}\,f_i(\mathbf{x}, t). \tag{40}$$

We can rewrite this in the conventional lattice Boltzmann form

$$\hat{f}_i(\mathbf{x}, t + n\Delta t) = \mathsf{S}\,\mathsf{C}\,\mathsf{S}\,\mathsf{C}\,\ldots\,\mathsf{S}\,\mathsf{C}\,\mathsf{S}\,\mathsf{C}\,\hat{f}_i(\mathbf{x}, t) \tag{41}$$

by defining the translated distribution functions

$$\hat{f}_i(\mathbf{x}, t) = (\mathsf{S}^{1/2}\,f_i)(\mathbf{x}, t) = f_i(\mathbf{x} - \tfrac{1}{2}\boldsymbol{\xi}_i\Delta t, t). \tag{42}$$

In a concrete implementation, we evaluate the macrosopic initial conditions at the half-points $\mathbf{x} - \frac{1}{2}\boldsymbol{\xi}_i\Delta t$ of the lattice, then translate the initial distributions onto the lattice points before performing a sequence of collision and streaming steps. This is easily done when the initial conditions are known analytic functions of $\mathbf{x}$, or could otherwise be done using linear interpolation. Finally, the distributions are linearly interpolated from the half points back to the lattice points, then summed to compute the macroscopic fields ρ, $\mathbf{u}$, $\mathbf{B}$ at lattice points for output. Interpolation is performed at most twice, regardless of the number of timesteps taken, so we can tolerate $O(\Delta t^2)$ interpolation errors while retaining global second-order accuracy.

Dellar [60] used the opposite splitting $\mathsf{C}^{1/2}\mathsf{S}\mathsf{C}^{1/2}$ and defined $\mathsf{C}^{1/2} = \frac{1}{2}(\mathsf{I} + \mathsf{C})$ to sufficient accuracy. The transformation $\overline{f}_i = \mathsf{C}^{-1/2} f_i$ is then the same change of variables introduced by He *et al.* [65] to construct an explicit scheme after integrating the unsplit discrete Boltzmann equation (28) along its characteristics for a time Δt. This alternative splitting requires no spatial interpolation, but instead requires the forward and backward half collision operators $\mathsf{C}^{\pm 1/2}$. The four lattice Boltzmann schemes described in this paper involve four different collision operators, and would hence require four different implementations of $\mathsf{C}^{\pm 1/2}$, while the linear interpolation of the distribution functions is common to them all. The two different splittings $\mathsf{S}^{1/2}\,\mathsf{C}\,\mathsf{S}^{1/2}$ and $\mathsf{C}^{1/2}\mathsf{S}\mathsf{C}^{1/2}$ produced similar numerical results, but the $\mathsf{S}^{1/2}\,\mathsf{C}\,\mathsf{S}^{1/2}$ splitting was much simpler to implement.

This construction of a lattice Boltzmann scheme from a discrete Boltzmann equation via Strang splitting is a standard piece of numerical analysis when taking Δt to zero for a fixed relaxation time τ. However, the lattice Boltzmann scheme remains a viable discretisation, in the sense that it still computes slowly-varying solutions of the discrete Boltzmann equation with second-order accuracy in Δt, when $\tau \ll \Delta t$. This relies on the Hénon correction, or equivalently the Crank–Nicholson discretisation, to keep the discrete collision step linearly stable when $\tau \ll \Delta t$, and a fortuitous cancellation between the Crank–Nicholson truncation error and the splitting error [60, 66].

D. Implementing collisions using moments

The streaming steps are naturally performed by moving the f_i values to adjacent lattice points. However, the collision steps is more easily performed using a basis of moments, such as ρ, $\mathbf{u}$, $\boldsymbol{\Pi}$, followed by reconstructing the post-collisional f_i from the post-collisional moments using the analogue of (29). In fact, we do not need to form the $f_i^{(0)}$, R_i, or Ω_{ij} explicitly. If a prime denotes a post-collisional value, as before, and we treat the body force $\mathbf{F}$ as independent of time for simplicity, then the post-collisional density and momentum are given by

$$\rho' = \rho, \quad \rho'\mathbf{u}' = \rho\mathbf{u} + \Delta t\mathbf{F}. \tag{43}$$

Taking the second moment of (33) gives

$$\partial_t\boldsymbol{\Pi} = -\frac{1}{\tau}\left(\boldsymbol{\Pi} - \boldsymbol{\Pi}^{(0)}\right) + \mathbf{F}\mathbf{u} + \mathbf{u}\mathbf{F} \tag{44}$$

by construction. We can now decompose $\boldsymbol{\Pi} = \boldsymbol{\Pi}^{(0)} + \boldsymbol{\Pi}^{(\mathrm{neq})}$ into its equilibrium and non-equilibrium parts. We know that $\partial_t\boldsymbol{\Pi}^{(0)} = \mathbf{F}\mathbf{u} + \mathbf{u}\mathbf{F}$ for evolution under (33), which leaves

$$\partial_t\boldsymbol{\Pi}^{(\mathrm{neq})} = -\frac{1}{\tau}\boldsymbol{\Pi}^{(\mathrm{neq})}. \tag{45}$$

Solving this with the Crank–Nicolson discretisation

$$\boldsymbol{\Pi}'^{(\mathrm{neq})} - \boldsymbol{\Pi}^{(\mathrm{neq})} = -\frac{\Delta t}{2\tau}\left(\boldsymbol{\Pi}'^{(\mathrm{neq})} + \boldsymbol{\Pi}^{(\mathrm{neq})}\right) \tag{46}$$

gives

$$\boldsymbol{\Pi}'^{(\mathrm{neq})} = \frac{\tau - \Delta t/2}{\tau + \Delta t/2}\,\boldsymbol{\Pi}^{(\mathrm{neq})}. \tag{47}$$

The complete post-collisional momentum flux is

$$\boldsymbol{\Pi}' = \boldsymbol{\Pi}'^{(0)} + \frac{\tau - \Delta t/2}{\tau + \Delta t/2}\,\left(\boldsymbol{\Pi} - \boldsymbol{\Pi}^{(0)}\right). \tag{48}$$

This corresponds to the second moment of Kupershtokh's exact difference method for implementing body forces [67, 68]. One can also derive (48) directly from a Crank–Nicolson discretisation of (44) without forming (45) analytically [64]. Finally, we relax the remaining degrees of freedom using the relaxation time τ, and then reconstruct the post-collisional distribution functions from the post-collisional moments [69].

IV. Lattice Boltzmann magnetohydrodynamics

To construct a lattice Boltzmann scheme for magnetohydrodynamics we need to incorporate the effect of the magnetic field on the fluid, and also evolve the magnetic field. We can incorporate the Maxwell stress from (10) by changing the equilibrium momentum flux to

$$\boldsymbol{\Pi}^{(0)} = \theta\rho\mathbf{I} + \rho\mathbf{u}\mathbf{u} + \frac{1}{2}|\mathbf{B}|^2\,\mathbf{I} - \mathbf{B}\mathbf{B}. \tag{49}$$

The $f_i^{(0)}$ given by(29) now depend on ρ, $\mathbf{u}$, and $\mathbf{B}$. This hydrodynamic lattice Boltzmann scheme will reproduce the ideal MHD momentum equation in its momentum-conserving form at leading order. There will be small errors in the viscous stress from the extra terms in $\nabla\cdot\boldsymbol{\Pi}^{(0)}$ in (24). These will be comparable to the existing $\nabla\cdot(\rho\mathbf{u}\mathbf{u}\mathbf{u})$ error when the Alfvén speed $|\mathbf{B}|/\sqrt{\rho}$ is comparable to $|\mathbf{u}|$.

The evolution of the magnetic field is more difficult to simulate using a kinetic formulation. We can rewrite Faraday's law in divergence form as

$$\partial_t\mathbf{B} + \nabla\cdot\boldsymbol{\Lambda} = 0 \tag{50}$$

by introducing a tensor $\boldsymbol{\Lambda}$ with components $\Lambda_{\alpha\beta} = -\epsilon_{\alpha\beta\gamma}E_\gamma$. This now resembles the momentum equation in (20a), except the momentum flux tensor $\boldsymbol{\Pi}$ is symmetric by construction, while the electric field tensor $\boldsymbol{\Lambda}$ should be antisymmetric. It is thus impossible to recover (50) by representing $\mathbf{B}$ as the first moment of some scalar distribution functions, analogous to our representation of the momentum vector $\rho\mathbf{u}$ in (27).

Instead, we introduce a set of M vector-valued distribution functions $\mathbf{g}_i(\mathbf{x}, t)$, and represent $\mathbf{B}$ and $\boldsymbol{\Lambda}$ by [25]

$$\mathbf{B} = \sum_{i=0}^{M-1}\mathbf{g}_i, \quad \boldsymbol{\Lambda} = \sum_{i=0}^{M-1}\boldsymbol{\xi}_i\mathbf{g}_i. \tag{51}$$

This representation of $\boldsymbol{\Lambda}$ is not constrained to be either symmetric or antisymmetric. We can typically choose M smaller than N, and so use fewer discrete velocities to represent the magnetic field than we used in sect. III to represent the hydrodynamic variables. For example, Fig. 1 shows the discrete velocities used in a two-dimensional formulation with nine velocities for the hydrodynamic variables, but just five velocities for the electromagnetic variables.

We postulate that the $\mathbf{g}_i$ evolve according to a kinetic equation of the form

$$\partial_t\mathbf{g}_i + \boldsymbol{\xi}_i\cdot\nabla\mathbf{g}_i = -\sum_{j=0}^{M-1}\mathbf{L}_{ij}\left(\mathbf{g}_j - \mathbf{g}_j^{(0)}\right). \tag{52}$$

This collision operator involves an indexed set of 3×3 matrices $\mathbf{L}_{ij}$ because $\mathbf{g}_i$ and $\mathbf{g}_j$ are themselves 3-component

vectors. We choose the $\mathbf{g}_i^{(0)}$ and the L_{ij} so that taking the zeroth and first moments of (52) gives (50) and

$$\partial_t \mathbf{\Lambda} + \nabla\cdot\mathbf{M} = -\frac{1}{\tau_{\mathbf{\Lambda}}}\left(\mathbf{\Lambda} - \mathbf{\Lambda}^{(0)}\right), \tag{53}$$

where the second moment of the $\mathbf{g}_i$ is

$$\mathbf{M} = \sum_{i=0}^{M-1} \boldsymbol{\xi}_i \boldsymbol{\xi}_i \mathbf{g}_i. \tag{54}$$

In other words, $\mathbf{\Lambda}$ is an eigenfunction of the collision operator on the right-hand side of (52) with eigenvalue $-1/\tau_{\mathbf{\Lambda}}$, just as we required $\mathbf{\Pi}$ to be an eigenfunction of the hydrodynamic collision operator with eigenvalue $-1/\tau$ in deriving (23).

If we choose $\mathbf{\Lambda}^{(0)} = \mathbf{uB} - \mathbf{Bu}$ and the equilibrium distributions

$$\mathbf{g}_i^{(0)} = W_i\left(\mathbf{B} + \Theta^{-1}\boldsymbol{\xi}_i \cdot \mathbf{\Lambda}^{(0)}\right), \tag{55}$$

with suitable weights W_i, we recover the ideal MHD induction equation $\partial_t\mathbf{B} = \nabla\times(\mathbf{u}\times\mathbf{B})$ at leading order for solutions that vary slowly on timescales much longer than $\tau_{\mathbf{\Lambda}}$. The lattice constant Θ is defined by the isotropy condition

$$\sum_{i=0}^{M-1} W_i \boldsymbol{\xi}_i \boldsymbol{\xi}_i = \Theta\mathbf{I} \tag{56}$$

for the discrete velocities $\boldsymbol{\xi}_i$. The components of the second moment of the equilibrium distributions are then

$$M^{(0)}_{\alpha\beta\gamma} = \sum_{i=0}^{M-1} \xi_{i\alpha}\xi_{i\beta}g^{(0)}_{i\gamma} = \Theta\delta_{\alpha\beta}B_\gamma. \tag{57}$$

The weights for the five discrete velocities shown in Fig. 1 are $W_0 = 1/3$, and $W_i = 1/6$ for $i = 1, 2, 3, 4$. These weights give $\Theta = 1/3$.

Posing a multiple-scales expansion of $\mathbf{\Lambda} = \mathbf{\Lambda}^{(0)} + \mathbf{\Lambda}^{(1)} + \cdots$, $\mathbf{M} = \mathbf{M}^{(0)} + \mathbf{M}^{(0)} + \cdots$, and $\partial_t = \partial_{t_0} + \partial_{t_1} + \cdots$ as in Sec. III in the evolution equation (53) for $\mathbf{\Lambda}$ gives at leading order:

$$\mathbf{\Lambda}^{(1)} = -\tau_{\mathbf{\Lambda}}\left(\nabla\cdot\mathbf{M}^{(0)} + \partial_{t_0}\mathbf{\Lambda}^{(0)}\right) = -\tau_{\mathbf{\Lambda}}\Theta\left(\nabla\mathbf{B} + O(\mathrm{Ma}^3)\right). \tag{58}$$

The $O(\mathrm{Ma}^3)$ estimate for $\partial_{t_0}\mathbf{\Lambda}^{(0)}$ comes from assuming that the Alfvén velocity $\mathbf{B}/\sqrt{\rho}$ is comparable to the fluid velocity $\mathbf{u}$. Neglecting the $O(\mathrm{Ma}^3)$ error term in (58) leads to a resistive MHD induction equation in the form

$$\partial_t\mathbf{B} = \nabla\times(\mathbf{u}\times\mathbf{B}) + \tau_{\mathbf{\Lambda}}\Theta\nabla^2\mathbf{B}. \tag{59}$$

This agrees with (6) with resistivity $\eta = \tau_{\mathbf{\Lambda}}\Theta$, but without the $\mathbf{u}\nabla\cdot\mathbf{B}$ term.

The expression (58) for $\mathbf{\Lambda}^{(1)}$ is not antisymmetric. The symmetric part leads to the parabolic divergence-cleaning term $\nabla(\eta\nabla\cdot\mathbf{B})$ in (6). Moreover, since $\mathbf{\Lambda}^{(0)}$ is antisymmetric, and hence has trace zero, we can use

$$\mathrm{Tr}\,\mathbf{\Lambda} = \mathrm{Tr}\,\mathbf{\Lambda}^{(0)} + \mathrm{Tr}\,\mathbf{\Lambda}^{(1)} + \cdots = -\tau_{\mathbf{\Lambda}}\Theta\nabla\cdot\mathbf{B} + O(\tau_{\mathbf{\Lambda}}{}^2) \tag{60}$$

as a consistent approximation for $\nabla\cdot\mathbf{B}$ that is compatible with the kinetic representation of the magnetic field [25, 27]. The $O(\mathrm{Ma}^3)$ contribution from $\partial_{t_0}\mathbf{\Lambda}^{(0)}$ in (58) and the $O(\tau_{\mathbf{\Lambda}}{}^2)$ contribution from $\mathbf{\Lambda}^{(2)}$ both have trace zero, so neither appears in (60).

More generally, we can specify the matrices L_{ij} implicitly by specifying how the right hand side of (52) should act on a basis of moments of the $\mathbf{g}_i$. For the five discrete velocites in two dimensions shown in Fig. 1, or the analogous set of seven discrete velocities in three dimensions, the moments $\mathbf{B}$, $\mathbf{\Lambda}$, $\mathbf{M}$ form a basis [26, 27]. The components $M_{\alpha\beta\gamma}$ are identically zero unless $\alpha = \beta$ for these sets of discrete velocities, so $\mathbf{B}$, $\mathbf{\Lambda}$, $\mathbf{M}$ comprise $2 + 4 + 4 = 10$ degrees of freedom in two dimensions, and $3 + 9 + 9 = 21$ degrees of freedom in three dimensions. We can thus implement the collision operator appearing on the right-hand side of (52) by relaxing these different moments, then reconstructing the post-collisional distributions using [26, 27]

$$g_{i\beta} = \tfrac{1}{2}\left(\xi_{i\alpha}\Lambda_{\alpha\beta} + \xi_{i\gamma}\xi_{i\alpha}M_{\gamma\alpha\beta}\right) \text{ for } i \neq 0, \quad g_{0\beta} = B_\beta - M_{\alpha\alpha\beta}, \tag{61}$$

with an implied summation over repeated Greek indices. There is no need to construct the matrices $\mathbf{L}_{ij}$ explicitly.

V. Implementing 8-wave magnetohydrodynamics

To implement the various formulations of 8-wave magnetohydrodynamics we need to add source terms proportional to $\nabla\cdot\mathbf{B}$ to the induction equation, and sometimes also to the momentum equation, so they become

$$\partial_t(\rho\mathbf{u}) + \nabla\cdot\mathbf{\Pi} = \mathbf{F}, \quad \partial_t\mathbf{B} + \nabla\cdot\mathbf{\Lambda} = \mathbf{G}. \tag{62}$$

There are now source terms $\mathbf{F}$ and $\mathbf{G}$ as well as divergences of fluxes $\mathbf{\Pi}$ and $\mathbf{\Lambda}$. As in Sec. III, we need to add corresponding source terms to the evolution equations for these fluxes,

$$\partial_t\mathbf{\Pi} + \nabla\cdot\mathbf{Q} = -\frac{1}{\tau}\left(\mathbf{\Pi} - \mathbf{\Pi}^{(0)}\right) + \mathbf{Fu} + \mathbf{uF}, \tag{63a}$$

$$\partial_t\mathbf{\Lambda} + \nabla\cdot\mathbf{M} = -\frac{1}{\tau_\Lambda}\left(\mathbf{\Lambda} - \mathbf{\Lambda}^{(0)}\right) + \frac{1}{\rho}(\mathbf{FB} - \mathbf{BF}) + \mathbf{uG} - \mathbf{Gu}, \tag{63b}$$

so that the contributions from the source terms $\mathbf{F}$ and $\mathbf{G}$ cancel in the evolution equations for $\mathbf{\Pi}^{(\mathrm{neq})}$ and $\mathbf{\Lambda}^{(\mathrm{neq})}$ that determine the viscous stress and the resistive electric field. The right-hand side of the evolution equation for $\mathbf{\Lambda}$ in (63b) comes from considering $\partial_t\mathbf{\Lambda}^{(0)}$. This calculation is slightly neater if we use the alternating tensor $\boldsymbol{\epsilon}$ with components $\epsilon_{\alpha\beta\gamma}$ to form the antisymmetric tensor $\mathbf{\Lambda}^{(0)} = \mathbf{uB} - \mathbf{Bu} = \boldsymbol{\epsilon}\cdot(\mathbf{u}\times\mathbf{B})$ from the vector $\mathbf{u}\times\mathbf{B}$. We then just need to consider

$$\partial_t(\mathbf{u}\times\mathbf{B}) = (\partial_t\mathbf{u})\times\mathbf{B} + \mathbf{u}\times(\partial_t\mathbf{B}) = \frac{1}{\rho}(\mathbf{F} - \nabla\cdot\mathbf{\Pi})\times\mathbf{B} + \mathbf{u}\times(\mathbf{G} - \nabla\cdot\mathbf{\Lambda}), \tag{64}$$

and contract with $\boldsymbol{\epsilon}$ to form the right-hand side of (63b). As in Sec. III, these algebraic terms can be elegantly implemented in a discrete approximation to (63a,b) using the moment form of the exact different method [64, 67, 68]

$$\mathbf{\Pi}' = \mathbf{\Pi}'^{(0)} + \frac{\tau - \Delta t/2}{\tau + \Delta t/2}\left(\mathbf{\Pi} - \mathbf{\Pi}^{(0)}\right), \tag{65}$$

and

$$\mathbf{\Lambda}' = \mathbf{\Lambda}'^{(0)} + \frac{\tau_\Lambda - \Delta t/2}{\tau_\Lambda + \Delta t/2}\left(\mathbf{\Lambda} - \mathbf{\Lambda}^{(0)}\right), \tag{66}$$

where a prime denotes the post-collisional value of a variable. Moreover, the source contributions to the evolution equation for $\mathbf{\Lambda}$ in (64) vanish exactly for the two simplest 8-wave variants, because $\mathbf{G}$ is parallel to $\mathbf{u}$, and $\mathbf{F}$ is either zero or parallel to $\mathbf{B}$. A good discretisation will preserve this qualitative property, leaving $\mathbf{\Lambda}'^{(0)} = \mathbf{\Lambda}^{(0)}$ exactly unchanged.

A. Hamiltonian 8-wave formulation

The Hamiltonian 8-wave formulation changes the induction equation to

$$\partial_t\mathbf{B} + \nabla\cdot\mathbf{\Lambda} = -\mathbf{u}\nabla\cdot\mathbf{B}, \tag{67}$$

while leaving the momentum equation unchanged. The equilibrium electric field tensor $\mathbf{\Lambda}^{(0)}$ has trace zero, so we can define $\Lambda = \mathrm{Tr}(\mathbf{\Lambda} - \mathbf{\Lambda}^{(0)}) = \mathrm{Tr}\,\mathbf{\Lambda}$ to give a consistent approximation to $\nabla\cdot\mathbf{B} \approx -(\mathrm{Tr}\,\mathbf{\Lambda})/(\tau_\Lambda\Theta)$ without knowing $\mathbf{u}$ and $\mathbf{B}$. We can thus approximate (67) by

$$\partial_t\mathbf{B} + \nabla\cdot\mathbf{\Lambda} = \frac{1}{\tau_\Lambda\Theta}\,\mathbf{u}\,\mathrm{Tr}\,\mathbf{\Lambda}. \tag{68}$$

Using the Strang splitting approach, we just need to incorporate this right-hand side in the discrete collision step. The Crank–Nicolson discretisation for colliding Λ is

$$\frac{1}{\Delta t}(\Lambda' - \Lambda) = -\frac{1}{2\tau_\Lambda}(\Lambda' + \Lambda), \tag{69}$$

where $\Lambda' = \Lambda(t + \Delta t)$ is the post-collisional value, and Λ without an argument is the pre-collisional value $\Lambda(t)$. We can solve this for

$$\Lambda' = \frac{\tau_{\mathbf{\Lambda}} - \Delta t/2}{\tau_{\mathbf{\Lambda}} + \Delta t/2}\,\Lambda, \tag{70}$$

and then form an approximation for $\Lambda(t + \Delta t/2)$ at the mid-point of the timestep,

$$\widetilde{\Lambda} = \frac{1}{2}\,(\Lambda' + \Lambda) = \frac{\tau_{\mathbf{\Lambda}}}{\tau_{\mathbf{\Lambda}} + \Delta t/2}\,\Lambda. \tag{71}$$

There is no source term in the momentum equation in the Hamiltonian 8-wave formulation, so the fluid velocity $\mathbf{u}$ remains unchanged in the collision step. The Crank–Nicolson discretisation of the right-hand side of (68) is thus

$$\frac{1}{\Delta t}\,(\mathbf{B}' - \mathbf{B}) = \frac{1}{\tau_{\mathbf{\Lambda}}\Theta}\widetilde{\Lambda}\mathbf{u}, \tag{72}$$

with solution

$$\mathbf{B}' = \mathbf{B} + \frac{\Delta t}{\tau_{\mathbf{\Lambda}}\Theta}\widetilde{\Lambda}\mathbf{u} = \mathbf{B} + \frac{\Delta t}{\tau_{\mathbf{\Lambda}} + \Delta t/2}(\mathrm{Tr}\,\mathbf{\Lambda})\mathbf{u}. \tag{73}$$

This leaves $\mathbf{\Lambda}^{(0)}$ unchanged, because $\mathbf{u}'\times\mathbf{B}' = \mathbf{u}\times\mathbf{B}' = \mathbf{u}\times\mathbf{B}$.

B. Symmetrisable 8-wave formulation

In Powell's and Godunov's symmetrisable 8-wave formulation we also add a source term to the momentum equation,

$$\partial_t\mathbf{B} + \nabla\cdot\mathbf{\Lambda} = -\mathbf{u}\nabla\cdot\mathbf{B}, \quad \partial_t(\rho\mathbf{u}) + \nabla\cdot\mathbf{\Pi} = -\mathbf{B}\nabla\cdot\mathbf{B}, \tag{74}$$

and approximate $\nabla\cdot\mathbf{B}$ by $-(\mathrm{Tr}\,\mathbf{\Lambda})/(\tau_{\mathbf{\Lambda}}\Theta)$ as before. We discretise the coupled evolution under the right-hand sides of (74) using

$$\frac{1}{\Delta t}\,(\mathbf{B}' - \mathbf{B}) = \frac{1}{2\tau_{\mathbf{\Lambda}}\Theta}\widetilde{\Lambda}(\mathbf{u}' + \mathbf{u}), \quad \frac{1}{\Delta t}\,(\mathbf{u}' - \mathbf{u}) = \frac{1}{2\tau_{\mathbf{\Lambda}}\Theta}\frac{1}{\rho}\widetilde{\Lambda}(\mathbf{B}' + \mathbf{B}), \tag{75}$$

where $\widetilde{\Lambda} = \frac{1}{2}(\Lambda' + \Lambda)$ as above. This factorised Crank–Nicolson discretisation is a convenient consistent approximation to the standard Crank–Nicolson discretisation, because

$$\frac{1}{2}\,(\Lambda'\,\mathbf{B}' + \Lambda\,\mathbf{B}) = \frac{1}{2}\,(\Lambda' + \Lambda)\,\frac{1}{2}\,(\mathbf{B}' + \mathbf{B}) + O(\Delta t^2), \tag{76}$$

and similarly for $\mathbf{u}$. We can rewrite (75) more compactly as

$$\mathbf{B}' - \mathbf{B} = \lambda(\mathbf{u}' + \mathbf{u}), \quad \rho(\mathbf{u}' - \mathbf{u}) = \lambda(\mathbf{B}' + \mathbf{B}), \tag{77}$$

by introducing the scaled divergence $\lambda = \widetilde{\Lambda}\Delta t/(2\tau_{\mathbf{\Lambda}}\Theta)$, and solve for

$$\mathbf{B}' = \mathbf{B} + 2\lambda\frac{\rho\mathbf{u} + \lambda\mathbf{B}}{\rho - \lambda^2}, \quad \mathbf{u}' = \mathbf{u} + 2\lambda\frac{\mathbf{B} + \lambda\mathbf{u}}{\rho - \lambda^2}. \tag{78}$$

This solution also satisfies $\mathbf{u}'\times\mathbf{B}' = \mathbf{u}\times\mathbf{B}$ so $\mathbf{\Lambda}'^{(0)} = \mathbf{\Lambda}^{(0)}$ is unchanged. This exact property of the solution is one reason to prefer the factorised Crank–Nicolson discretisation on the right-hand side of (76) over the more conventional discretisation on the left-hand side of (76).

C. Full Lorentz force through collisions

The third variant that we consider implements the full Lorentz force $(\nabla\times\mathbf{B})\times\mathbf{B}$ through the collision operator using $\nabla\times\mathbf{B}$ obtained from the non-equilibrium part of the magnetic distribution functions [28, 30]. We previously included the Maxwell stress in the equilibrium momentum flux, and just added the correction term $-\mathbf{B}\nabla\cdot\mathbf{B}$ through the collision operator. The third variant solves

$$\partial_t\mathbf{B} + \nabla\cdot\mathbf{\Lambda} = \frac{1}{\tau_{\mathbf{\Lambda}}\Theta}\mathbf{u}\;\mathrm{Tr}\,\mathbf{\Lambda}, \quad \partial_t(\rho\mathbf{u}) + \nabla\cdot\mathbf{\Pi} = -\frac{1}{\tau_{\mathbf{\Lambda}}\Theta}\left(\boldsymbol{\epsilon} : \mathbf{\Lambda}^{(\mathrm{neq})}\right)\times\mathbf{B}, \tag{79}$$

where $\mathbf{\Pi}$ now omits the Maxwell stress. In index notation, the right-hand side of the momentum equation is

$$\frac{1}{\tau_{\mathbf{\Lambda}}\Theta}\left(\Lambda^{(\mathrm{neq})}_{\alpha\beta} - \Lambda^{(\mathrm{neq})}_{\beta\alpha}\right) B_\beta = \left[(\nabla\times\mathbf{B})\times\mathbf{B}\right]_\alpha \left(1 + O(\mathrm{Ma}^2)\right). \tag{80}$$

The $O(\mathrm{Ma}^2)$ relative error is due to $\partial_{t_0}\mathbf{\Lambda}^{(0)}$ as described in Sec. IV and at the end of this section.

We evolve $\mathbf{u}$ and $\mathbf{B}$ together in the collision step using the factorised Crank–Nicolson discretisation

$$\frac{1}{\Delta t}\left(\mathbf{B}' - \mathbf{B}\right) = \frac{1}{2\tau_{\mathbf{\Lambda}}\Theta}\widetilde{\Lambda}(\mathbf{u}' + \mathbf{u}), \quad \frac{1}{\Delta t}\left(\mathbf{u}' - \mathbf{u}\right) = \frac{1}{2}\frac{1}{\rho}\widetilde{\mathbf{J}}\times(\mathbf{B}' + \mathbf{B}), \tag{81}$$

with $\widetilde{\Lambda}$ as before, and the approximate current at the mid-point of the timestep

$$\widetilde{\mathbf{J}} = -\frac{1}{2\Theta\tau_{\mathbf{\Lambda}}}\boldsymbol{\epsilon} : \left(\mathbf{\Lambda}'^{(\mathrm{neq})} + \mathbf{\Lambda}^{(\mathrm{neq})}\right) = -\frac{1}{\Theta}\frac{\tau_{\mathbf{\Lambda}}}{\tau_{\mathbf{\Lambda}} + \Delta t/2}\ \boldsymbol{\epsilon} : \left(\mathbf{\Lambda} - \mathbf{\Lambda}^{(0)}\right). \tag{82}$$

We can write (81) more compactly as

$$\mathbf{B}' - \mathbf{B} = \lambda(\mathbf{u}' + \mathbf{u}), \quad \mathbf{u}' - \mathbf{u} = \mathcal{J}\times(\mathbf{B}' + \mathbf{B}), \tag{83}$$

by introducing $\lambda = \widetilde{\Lambda}\Delta t/(2\tau_{\mathbf{\Lambda}}\Theta)$ as before, and also the rescaled current $\mathcal{J} = \widetilde{\mathbf{J}}\Delta t/(2\rho)$. Eliminating $\mathbf{B}'$ gives the single equation

$$\mathbf{u}' - \mathbf{u} = 2\mathcal{J}\times\mathbf{B} + \lambda\mathcal{J}\times(\mathbf{u}' + \mathbf{u}). \tag{84}$$

This equation coincides with the mid-point rule discretisation in the Boris pusher algorithm [4] for a non-relativistic charged particle subjected to an effective electric field $2\mathcal{J}\times\mathbf{B}$ and an effective magnetic field $\lambda\mathcal{J}$. Its analytical solution is [4]

$$\mathbf{u}' = \mathbf{u} + \frac{2}{1 + \lambda^2|\mathcal{J}|^2}\mathcal{J}\times(\mathbf{B} + \lambda\mathbf{u} + \lambda\mathcal{J}\times(\mathbf{B} + \lambda\mathbf{u})). \tag{85}$$

Taking the inner product of (84) with $\mathbf{u}' + \mathbf{u}$ leads to [4]

$$|\mathbf{u}' - \mathcal{J}\times\mathbf{B}|^2 = |\mathbf{u} + \mathcal{J}\times\mathbf{B}|^2, \tag{86}$$

so the solution $\mathbf{u}'$ is equal to $\mathcal{J}\times\mathbf{B}$ plus a norm-preserving exact rotation of $\mathbf{u} + \mathcal{J}\times\mathbf{B}$. The exact solution of (84) thus equals the result of a Strang splitting that adds $\mathcal{J}\times\mathbf{B}$ twice, once before and once after solving the simplified version of (84) with $\mathbf{B} = 0$. These exact results arise from the factorised form of the Crank–Nicolson discretisation with a single λ and $\mathcal{J}$ evaluated at the mid-point of the time interval.

This formulation that includes the Lorentz force as a body force has the advantage that it leaves the viscous stress completely unchanged. The earlier formulations that include the Maxwell stress in $\mathbf{\Pi}^{(0)}$ introduce small errors into $\mathbf{\Pi}^{(1)}$ via the $\mathbf{u}(\nabla\cdot\mathbf{\Pi}^{(0)})$ and $(\nabla\cdot\mathbf{\Pi}^{(0)})\mathbf{u}$ terms in (24). These errors are comparable to the $\nabla\cdot(\rho\mathbf{uuu})$ error in $\mathbf{\Pi}^{(1)}$ due to the missing $\rho\mathbf{uuu}$ in the third moment $\mathbf{Q}^{(0)}$ of the discrete equilibria (29) on standard lattices.

However, the approximation of $\nabla\times\mathbf{B}$ using $\mathbf{\Lambda}^{(\mathrm{neq})} = \mathbf{\Lambda}^{(1)} + O(\tau_{\mathbf{\Lambda}}{}^2)$ introduces larger errors elsewhere. The contribution from $\partial_{t_0}\mathbf{\Lambda}^{(0)}$ vanishes in $\mathrm{Tr}\,\mathbf{\Lambda}$, but does not vanish in

$$\begin{aligned}
\boldsymbol{\epsilon} : \mathbf{\Lambda}^{(1)} &= -\tau_{\mathbf{\Lambda}}\boldsymbol{\epsilon} : \left(\Theta\nabla\mathbf{B} + \partial_{t_0}\mathbf{\Lambda}^{(0)}\right), \\
&= -\tau_{\mathbf{\Lambda}}\left(\Theta\nabla\times\mathbf{B} + 2\partial_{t_0}(\mathbf{u}\times\mathbf{B})\right), \\
&= -\tau_{\mathbf{\Lambda}}\Theta\nabla\times\mathbf{B} - 2\tau_{\mathbf{\Lambda}}\left((\partial_{t_0}\mathbf{u})\times\mathbf{B} + \mathbf{u}\times(\partial_{t_0}\mathbf{B})\right), \\
&= -\tau_{\mathbf{\Lambda}}\Theta\nabla\times\mathbf{B}\left(1 + O(\mathrm{Ma}^2)\right).
\end{aligned} \tag{87}$$

The relative error in the current, and hence the Lorentz force, is $O(\mathrm{Ma}^2)$, the same as the relative error in the viscous stress. However, the contribution from the viscous stress is divided by the Reynolds number, the ratio of inertial to viscous effects, which is typically large.

A more accurate implementation of the Lorentz force would include the Maxwell stress in $\mathbf{\Pi}^{(0)}$, but include compensating $\mathbf{u}(\mathbf{J}\times\mathbf{B})$ and $(\mathbf{J}\times\mathbf{B})\mathbf{u}$ terms in the evolution equation (44) for $\mathbf{\Pi}$. These small corrections to the viscous stress can be evaluated to sufficient accuracy using $\mathbf{\Lambda}^{(\mathrm{neq})}$.

D. Summary

Table 1 summarises the key differences between the three different schemes presented in the previous three subsections and the original vector lattice Boltzmann MHD scheme [25]. The schemes differ in whether they include a $\mathbf{u}\nabla\cdot\mathbf{B}$ term in the induction equation to restore Galilean invariance, and in how they implement the action of the magnetic field on the fluid. The original scheme included the Maxwell stress in the equilibrium distributions. This is modified in the symmetrisable scheme, and completely replaced in the Lorentz force scheme. Two of the schemes are named "Hamiltonian" and "symmetrisable" for brevity, although these properties only apply to their ideal forms with zero resistivity and zero viscosity.

Table 1 Summary of the different schemes

brief name	reference	Galilean invariant	momentum equation
original	[25]	no	Maxwell stress
Hamiltonian	V.A	yes	Maxwell stress
symmetrisable	V.B	yes	Maxwell stress plus $\mathbf{B}\nabla\cdot\mathbf{B}$
Lorentz force	V.C	yes	Lorentz force $\mathbf{J}\times\mathbf{B}$

VI. Numerical Experiments

The following numerical experiments establish firstly that the symmetrisable and Lorentz force schemes correctly implement the Lorentz force $\mathbf{J}\times\mathbf{B}$, which differs from the divergence of the Maxwell stress when $\nabla\cdot\mathbf{B}\neq 0$, and secondly that the divergence of the magnetic field is advected with the fluid velocity. We also simulate the Orszag–Tang vortex to demonstrate the robustness of Lorentz force scheme that use gradient information from the non-equilibrium magnetic distribution functions to implement the complete Lorentz force in the collision operator. In all cases, the magnetic distribution functions were initialised with $\mathbf{\Lambda}=\mathbf{\Lambda}^{(0)}-\tau_{\mathbf{\Lambda}}\Theta\nabla\mathbf{B}$ using the gradient of the initial magnetic field. The hydrodynamic and magnetic distribution functions were evaluated using the initial conditions at the half points, as described in Sec. III.C. The output distribution functions were later interpolated back onto lattice points before being summed to reconstruct the macroscopic fields. All the numerical experiments were performed using periodic boundary conditions.

A. A purely divergent magnetic field

We consider initial conditions with the fluid at rest with uniform density $\rho=\rho_0$, and an initial magnetic field $\mathbf{B}=B(x)\hat{\mathbf{x}}$. This is a completely artificial magnetic field that is purely divergent, designed to test this aspect of the various numerical schemes. The divergence of the Maxwell stress for this field creates a magnetic tension $-BB'$ in the x-direction that generates a flow, although the current $\nabla\times\mathbf{B}$ and Lorentz force $(\nabla\times\mathbf{B})\times\mathbf{B}$ are identically zero.

For small perturbations to a uniform field, the MHD equations as solved by the original lattice Boltzmann scheme

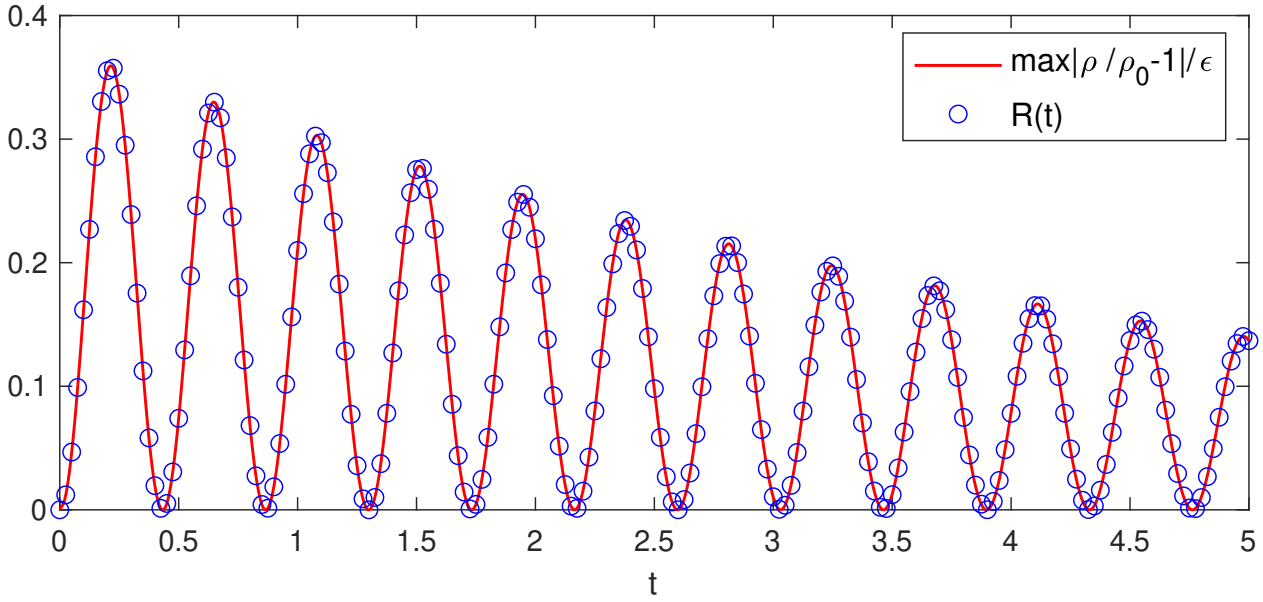

Fig. 2 Evolution of the density in the original scheme due to the non-vanishing Maxwell stress.

have an analytical solution of the form

$$\rho(x,t) = \rho_0\,(1 + \epsilon R(t)\sin(kx)) + O(\epsilon^2), \tag{88a}$$

$$\mathbf{u}(x,t) = \epsilon U(t)\cos(kx)\hat{\mathbf{x}} + O(\epsilon^2), \tag{88b}$$

$$\mathbf{B}(x,t) = B_0\left(1 + \epsilon\sin(kx)\exp(-\eta k^2 t)\right)\hat{\mathbf{x}}. \tag{88c}$$

These perturbations have constant wavenumber k and amplitude $\epsilon \ll 1$. The lattice Boltzmann schemes all include a parabolic divergence-cleaning term $\eta\nabla\nabla\cdot\mathbf{B}$ so this purely divergent magnetic field decays even though the current $\nabla\times\mathbf{B}$ is identically zero. The advective term $\nabla\times(\mathbf{u}\times\mathbf{B})$ is also identically zero, so (88c) holds exactly. The functions $R(t)$ and $U(t)$ satisfy the coupled ordinary differential equations

$$\frac{\mathrm{d}R}{\mathrm{d}t} = kU, \tag{89a}$$

$$\frac{\mathrm{d}U}{\mathrm{d}t} = -k\theta R - 2\nu k^2 U + k\exp(-\nu k^2 t)B_0^2/\rho_0, \tag{89b}$$

where $\nu = \mu/\rho$ is the kinematic viscosity. We choose initial conditions with $R(0) = 0$ and $U(0) = 0$. These linear, constant coefficient ordinary differential equations have an analytical solution. When $\nu = \eta$, this solution takes the particularly simple form

$$R(t) = \frac{B_0^2}{\rho_0(\theta - k^2\nu^2)}\left(1 - \cos\left(kt\sqrt{\theta - k^2\nu^2}\right)\right)\exp(-\nu k^2 t). \tag{90}$$

Figure 2 shows the evolution of the density perturbations over time in a numerical experiment using the original lattice Boltzmann scheme in the domain $[0, 1]$ with 512 lattice points, and the parameter values $k = 2\pi$, $\epsilon = 10^{-6}$, $\nu = \eta = 1/100$, $B_0 = \rho_0 = 1$, and Mach number $\mathrm{Ma} = \sqrt{3}/4$. The evolution of the rescaled spatial maximum of the density profile

$$\max_{x\,\in\,[0,1]}\left(\frac{1}{\epsilon}\left|\frac{\rho(x,t)}{\rho_0} - 1\right|\right) \tag{91}$$

is in good agreement with the analytical solution $R(t)$ in (90).

Figure 3 shows the equivalent time series computed with the symmetrisable scheme. In theory, the divergence of the Maxwell stress for this magnetic field should exactly balance the $-\mathbf{B}\nabla\cdot\mathbf{B}$ term in the momentum equation. However,

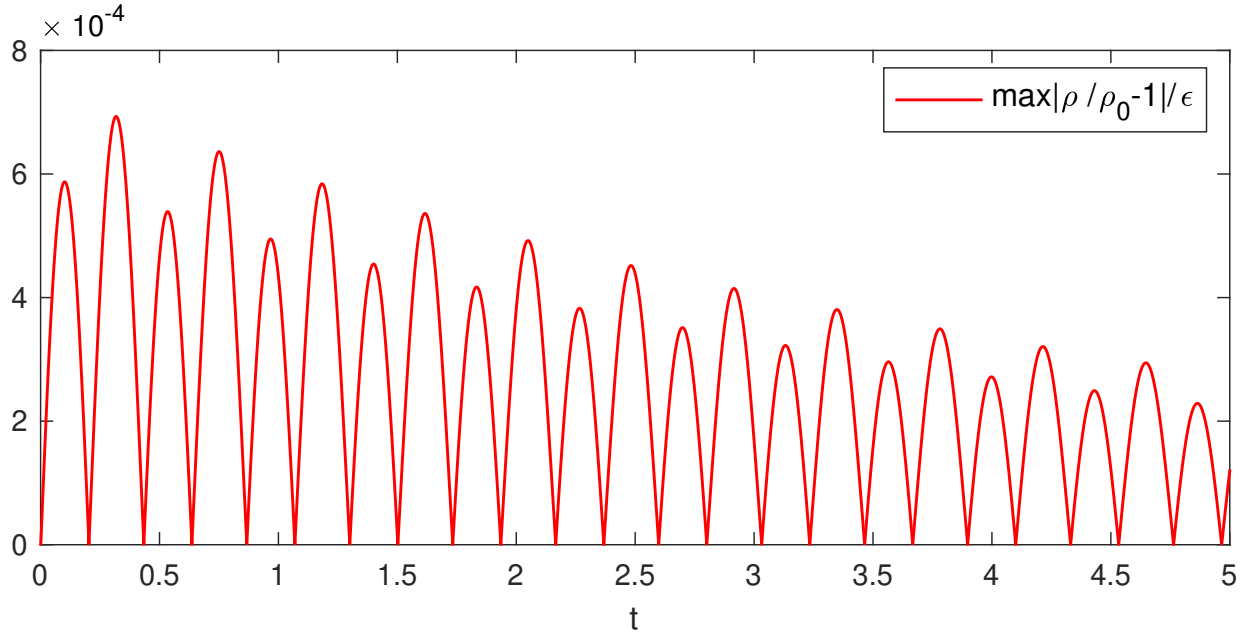

Fig. 3 Evolution of the density in the symmetrisable scheme with a compensating body force. Note the factor of 10^{-4} multiplying the vertical axis labels.

this balance is not perfect in the numerical experiment, because the product rule for differentiation only holds discretely to within the spatial truncation error, but the perturbations driven by the imbalance are about a factor of 500 smaller than those without the compensating $-\mathbf{B}\nabla\cdot\mathbf{B}$ term. They also have twice the frequency, reflecting their artificial origin. These perturbations have the same origin as the spurious mass currents in multiphase lattice Boltzmann simulations that are due to an imbalance between the pressure gradient ∇p and the product $\rho\nabla\mu$ of the density and the chemical potential gradient [70, 71]. The Lorentz force is identically zero for this magnetic field geometry, so the velocity and density perturbations remained zero to machine precision in numerical experiments with the Lorentz force scheme.

B. DeVore current-carrying cylinder

To see the behavior of a nonzero $\nabla\cdot\mathbf{B}$ in a more realistic scenario, we adopt a smoothed version of DeVore's [6] benchmark for a two-dimensional current-carrying cylinder. A magnetic field of the form

$$B_x = -yf(r), \quad B_y = xf(r), \quad r = \sqrt{x^2+y^2}, \tag{92}$$

corresponds to an axisymmetric current $J = \hat{\mathbf{z}}\cdot\nabla\times\mathbf{B} = rf'(r) + 2f(r)$ in the z direction. This magnetic field satisfies $\nabla\cdot\mathbf{B} = 0$ analytically, but any discrete approximation to $\nabla\cdot\mathbf{B}$ will be nonzero due to the spatial truncation error. We take f to be the smooth hperbolic tangent profile

$$f(r) = \frac{B_0}{2r_{\max}}\left(1+\tanh\left(\frac{r_{\max}-r}{\delta r}\right)\right). \tag{93}$$

DeVore [6] used a step function profile, and a scheme with flux limiters that could accommodate discontinuous initial conditions. All our lattice Boltzmann schemes solve the viscous and resistive MHD equations for smooth velocity and magnetic fields. All but the original scheme obtain information about the gradient of the magnetic field from the non-equilibrium parts of the magnetic distribution functions, so the initial magnetic field should be differentiable.

Figure 4 shows some results from numerical experiments with this initial magnetic field for the parameters $B_0 = 0.001$, $r_{\max} = 16$ and $\delta r = 1$ in a square domain with side length 100. The fluid velocity was set to be $\mathbf{u} = \hat{\mathbf{x}}$, a uniform stream in the x-direction. The viscosity and resistivity were $\nu = \eta = 0.001$, the Mach number $Ma = \sqrt{3}\times 0.0256$, and the lattice size 1024×1024. This weak magnetic field is approximately passive and exerts a negligible Lorentz

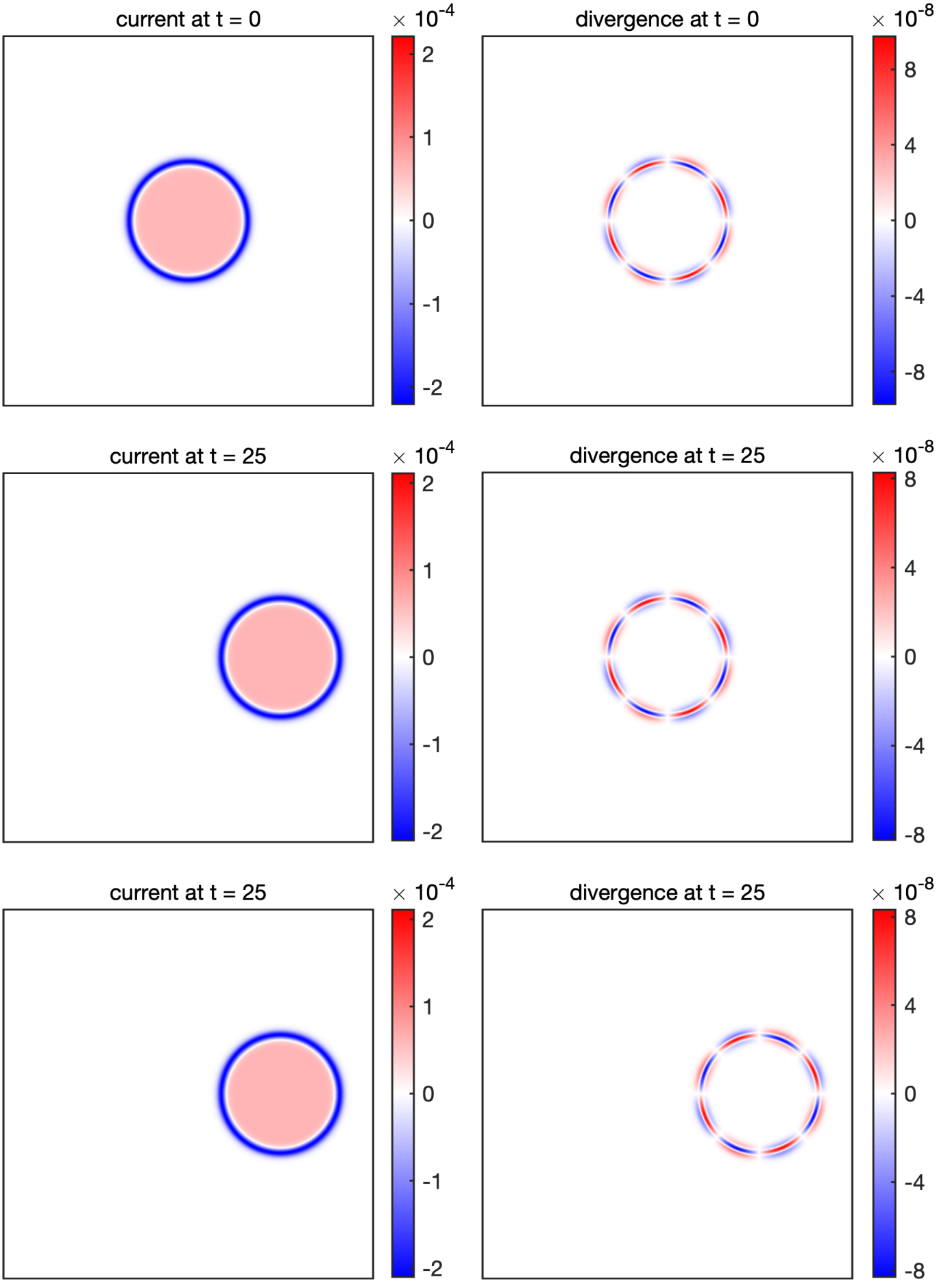

Fig. 4 Evolution of the current (left) and divergence (right) for an advected current-carrying cylinder. The top row shows the initial conditions. The middle and bottom rows show the solution at t = 25 using the orginal scheme (middle row) and the Hamiltonian scheme (bottom row).

force. The first row of plots show the initial current and divergence, computed using $\widetilde{J}$ and $\widetilde{\Lambda}$ as defined in Sec. V. The current appears axisymmetric as expected. The divergence, which is solely due to the spatial truncation error, shows an octopolar pattern due to the 4-fold rotational symmetry of the lattice.

The second row of plots in Fig. 4 shows the current and divergence at $t = 25$ computed using the original scheme. The current has been advected right by 25 spatial units, and slightly diffused through resistivity. The divergence has been diffused but not advected. The third row of plots shows the current and divergence at $t = 25$ computed using the Hamiltonian scheme. They confirm that the Hamiltonian scheme advects the divergence as well as the current.

C. Orszag–Tang vortex

The Orszag–Tang [72] vortex is a standard benchmark problem for two-dimensional incompressible MHD. The smooth initial conditions

$$u_x = 2\sin(y), \quad u_y = -2\sin(x), \quad b_x = 2\sin(2y), \quad b_y = -2\sin(x), \tag{94}$$

satisfy $\nabla\cdot\mathbf{B} = 0$ analytically. This flow evolves to create an intense current sheet surrounded by a vortex quadrupole. It occupies the domain $0 \le x, y \le 2\pi$ with periodic boundary conditions. The initial density field that ensures $\nabla\nabla : \mathbf{\Pi}^{(0)} = 0$ for an initially non-divergent fluid flow is

$$\rho = 1 + \frac{1}{\theta}\left\{4\cos(x)\left(\frac{4}{5}\cos(2y) - \cos(y)\right) - \frac{1}{2}|\mathbf{b}|^2\right\}. \tag{95}$$

Figure 5 shows the evolution of the vorticity and current for a numerical experiment with diffusivities $\eta = \nu = 1/200$ and Mach number $\mathrm{Ma} = \sqrt{3}\times 256\times 10^{-4}/\pi \approx 0.014$. The fluid and magnetic Reynolds numbers based on the domain size are thus both equal to $400\pi \approx 1257$. These plots were created from the velocity and magnetic fields computed on a 1024×1024 lattice using the Lorentz force scheme. The vorticity $\omega = \hat{\mathbf{z}}\cdot\nabla\times\mathbf{u}$ and current $J = \hat{\mathbf{z}}\cdot\nabla\times\mathbf{B}$ were computed by spectrally differentiating the $\mathbf{u}$ and $\mathbf{B}$ fields at lattice points.

Figure 6 shows the evolution of the maximum vorticity and maximum current over time. The results from the Lorentz force scheme and the original scheme are visually indistinguishable. The Lorentz force scheme was stable for simulating the same flow on a 512×512 lattice, while the other three scheme using the Maxwell stress were not.

Figure 7 shows that solutions computed with the symmetrisable and the Lorentz force schemes converge with second-order spatial accuracy towards reference solutions of the incompressible MHD equations under a diffusive scaling that lowers the Mach number with increasing spatial resolution. To be concrete, the numerical experiments with an $n\times n$ lattice was run with a Mach number $\mathrm{Ma} = \sqrt{3}\times 2^{18}\times 10^{-4}/(n\pi)$, giving $\mathrm{Ma} \approx 0.0035$ on the finest 4096×4096 lattice. A diffusive scaling is commonly used to approach the incompressible limit. The $O(\mathrm{Ma}^2)$ compressibility error then becomes $O(n^{-2})$ like the spatial truncation error. The prefactor in the Mach number was chosen to roughly balance the compressibility error with the truncation error, and to produce output at dimensionless time increments of 0.1 after an integer number of timesteps. Highly accurate reference solutions of the incompressible MHD equations were computed using a Fourier pseudo-spectral scheme on a 2048×2048 lattice with fourth-order Runge–Kutta timestepping. The maximum difference between these solutions and Fourier pseudo-spectral solutions on a coarser 1024×1024 lattice was less than 3×10^{-11}, much smaller than the differences shown in Fig. 7.

However, establishing second-order spatial convergence under diffusive scaling does not establish that the scheme is second-order accurate in time, because the timestep Δt scales like Δx^2. Tables 2 and 3 show the ℓ^2 and ℓ^∞ norms of the differences between the currents and vorticities computed by numerical experiments with different spatial resolutions at fixed Mach number $\mathrm{Ma} = \sqrt{3}\times 0.0256/\pi \approx 0.014$, and fixed fluid and magnetic Reynolds numbers. The empirical convergence order is defined by

$$\log_2\left(\frac{||F_{1024} - F_{2048}||}{||F_{2048} - F_{49096}||}\right), \tag{96}$$

where F_n is a field, either current or vorticity, computed on an $n\times n$ lattice, and $||\cdots||$ is either the ℓ^2 or the ℓ^∞ norm.

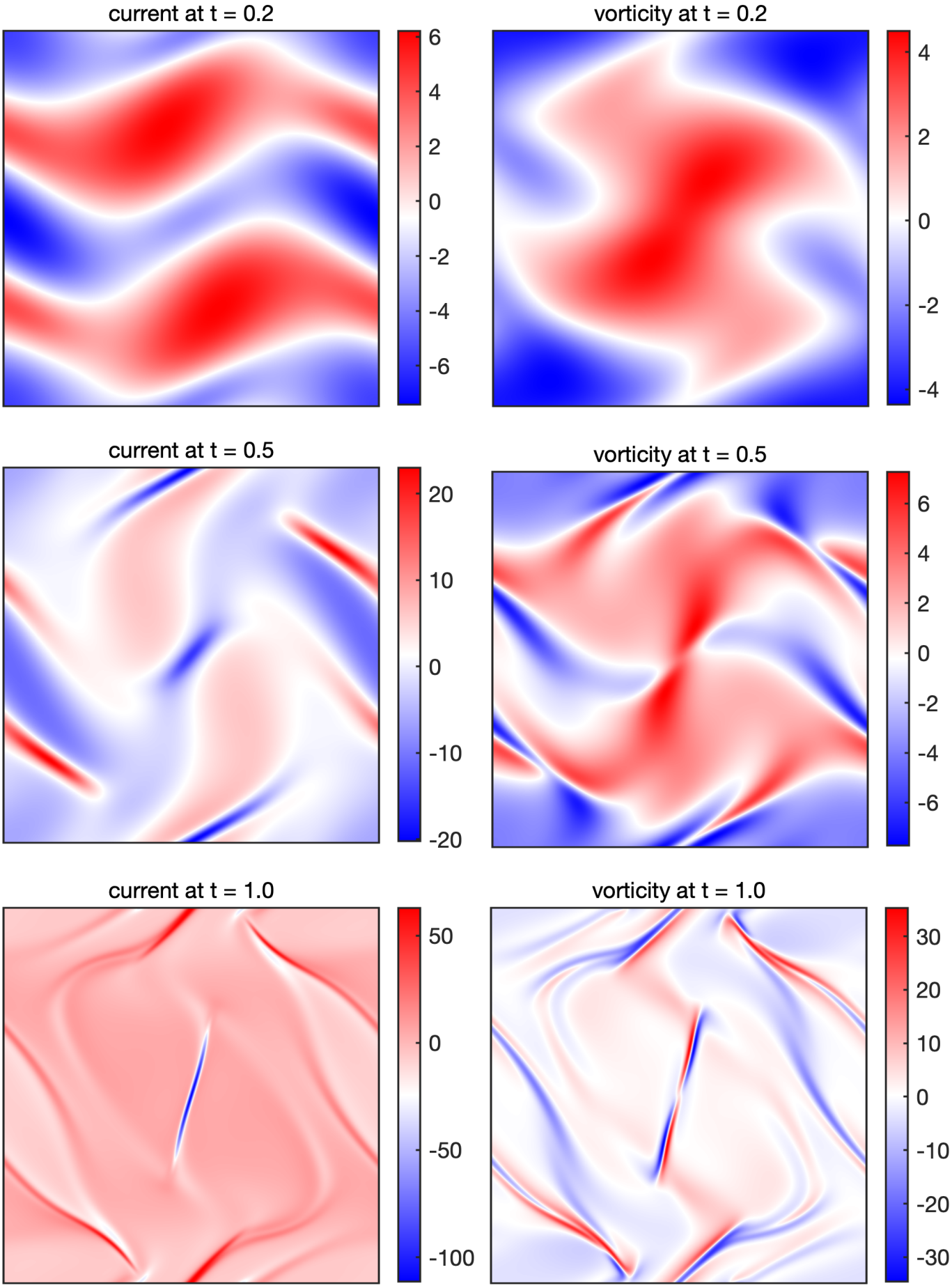

Fig. 5 **Evolution of the vorticity and current in the Orszag–Tang vortex simulated with the Lorentz force scheme.**

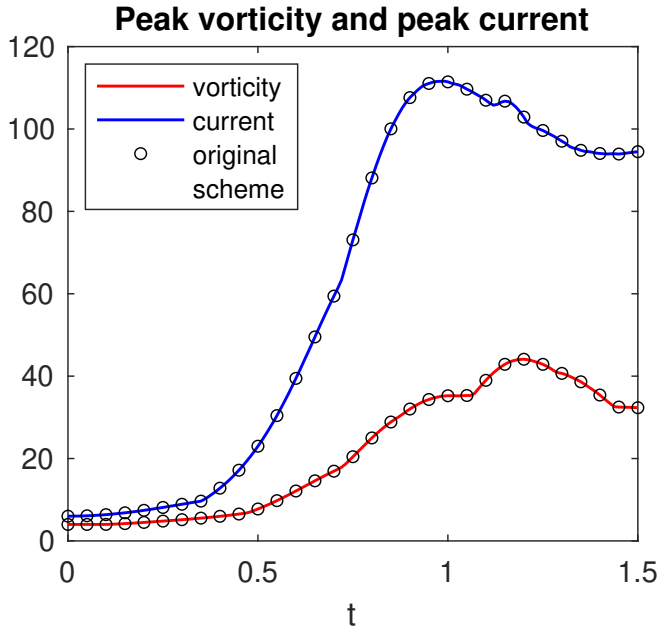

Fig. 6 Evolution of the peak vorticity and peak current in the Orszag–Tang vortex simulated using the Lorentz force scheme (lines) and the original scheme (circles).

The empirical convergence orders shown in Tables 2 and 3 are all consistent with the Hamiltonian, symmetrisable and Lorentz force schemes each having second-order accuracy in time. For these smooth initial conditions, and hence a very small initial discrete divergence, the data for the Hamiltonian and symmetrisable schemes were identical to the precision shown. The maximal differences in the vorticity and current fields were below 6×10^{-8} on the 1024×1024 lattice, dropping to below 3×10^{-9} on the 4096×4096 lattice.

However, the solution computed with the Lorentz force scheme does not converge to the same solution as the other three schemes under spatial refinement at fixed Mach number and fixed fluid and magnetic Reynolds numbers. Small differences persist around regions of high current and high vorticity, even for numerical experiments on 4096×4096 lattices, as shown in Fig. 8. This is consistent with the $O(\mathrm{Ma}^2)$ relative error in the current computed from $\boldsymbol{\epsilon} : \boldsymbol{\Lambda}^{(\mathrm{neq})}$ described in Sec. V.C. Compared with the other three schemes, the Lorentz force scheme has larger errors in the current but smaller errors in the vorticity.

Table 2 Convergence of the Hamiltonian and symmetrisable schemes

	$\|\|\Delta J\|\|_2$	$\|\|\Delta J\|\|_\infty$	$\|\|\Delta\omega\|\|_2$	$\|\|\Delta\omega\|\|_\infty$
1024 vs 2048	0.01522	0.28210	0.024591	0.75173
2048 vs 4096	0.00380	0.07017	0.006157	0.18903
empirical order	2.0032	2.0073	1.9978	1.9916

Table 3 Convergence of the Lorentz force scheme

	$\|\|\Delta J\|\|_2$	$\|\|\Delta J\|\|_\infty$	$\|\|\Delta\omega\|\|_2$	$\|\|\Delta\omega\|\|_\infty$
1024 vs 2048	0.02218	0.46647	0.01400	0.32015
2048 vs 4096	0.00549	0.11681	0.00348	0.07869
empirical order	2.0137	1.9976	2.0106	2.0246

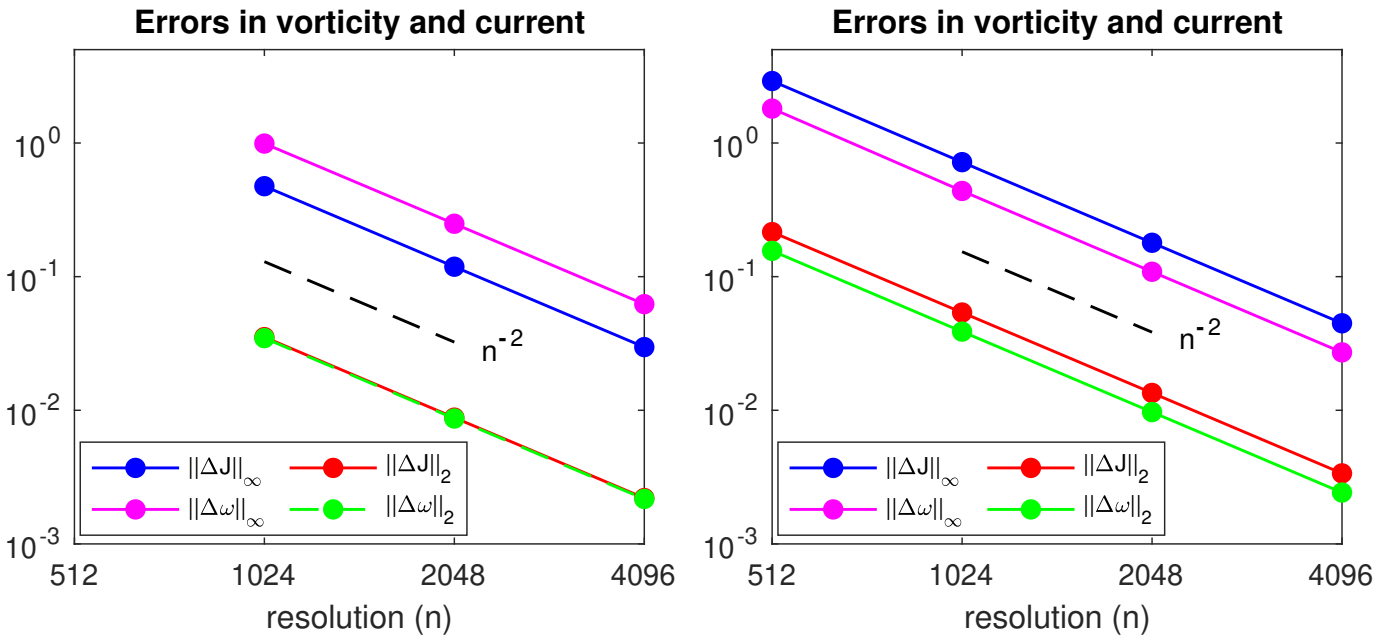

Fig. 7 ℓ^2 and ℓ^∞ differences in vorticity ω and current J between the symmetrisable scheme (left) or Lorentz force scheme (right) and the spectral reference solutions under diffusive scaling.

VII. Conclusions

Numerical algorithms for simulating MHD typically do not exactly preserve $\nabla\cdot\mathbf{B} = 0$. This can lead to artifacts in the computed solutions as structural properties of the MHD equations cease to hold [1–3]. There have been several approaches to include extra terms involving $\nabla\cdot\mathbf{B}$ to improve the structural properties of the MHD equations when $\nabla\cdot\mathbf{B} \neq 0$. These approaches are all based on an extended set of Maxwell equations that includes magnetic charges and magnetic currents. Dedner *et al.* [12] proposed that $\nabla\cdot\mathbf{B}$ should propagate and decay isotropically according to a telegraph equation, while Powell [13, 14] proposed that $\nabla\cdot\mathbf{B}$ should advect with the fluid velocity $\mathbf{u}$. The latter change brings the evolution equation for the magnetic field closer to a compressible variant of Jeffery's equation [35, 36] for evolving the orientations of axisymmetric particles in a suspension [38].

We have constructed lattice Boltzmann schems for several different variants of the MHD equations. They approximate $\nabla\cdot\mathbf{B}$ using the trace of the electric field tensor $\mathbf{\Lambda}$ constructed from the magnetic distribution functions. They all amend Faraday's law so that $\nabla\cdot\mathbf{B}$ advects with the fluid velocity $\mathbf{u}$, thus restoring Galilean invariance. The Hamiltonian variant makes this change alone. The symmetrisable hyperbolic variant also includes a $-\mathbf{B}\nabla\cdot\mathbf{B}$ force in the momentum equation, so that the force exerted by the magnetic field is the usual Lorentz force $(\nabla\times\mathbf{B})\times\mathbf{B}$ even when $\nabla\cdot\mathbf{B} \neq 0$. Finally, the Lorentz force variant omits the Maxwell stress from $\mathbf{\Pi}^{(0)}$ and includes the entire Lorentz force through the collision operator, approximating $\nabla\times\mathbf{B}$ using the non-equilibrium part of $\mathbf{\Lambda}$, as in [28]. The implementations of the symmetrisable and Lorentz force variants use a factorised Crank–Nicolson discretisation in the collision operator that exactly preserves qualitative properties. The symmetrisable variant exactly preserves the equilibrium electric field tensor $\mathbf{\Pi}^{(0)}$, consistent with the analytical properties of the source terms in the continuous time formulation (63b), and the Lorentz force variant exactly preserves the norm of the fluid velocity offset by the scaled Lorentz force, as in (86).

Numerical experiments confirm that $\nabla\cdot\mathbf{B}$ advects with the fluid velocity for all variants, and that the force exterted by the magnetic field is perpendicular to the magnetic field for the symmetrisable and Lorentz force variants. This holds exactly for the Lorentz force variant, and to a good approximation for the symmetrisable variant. The latter relies upon a cancellation between a term in the divergence of the Maxwell stress and the $\mathbf{B}\nabla\cdot\mathbf{B}$ term implemented in the collision operator. Having previously been employed for steady Hartmann flow [28], the Lorentz force scheme is stable enough to simulate the Orszag–Tang vortex [72], with results virtually indistinguishable from the original lattice Boltzmann MHD

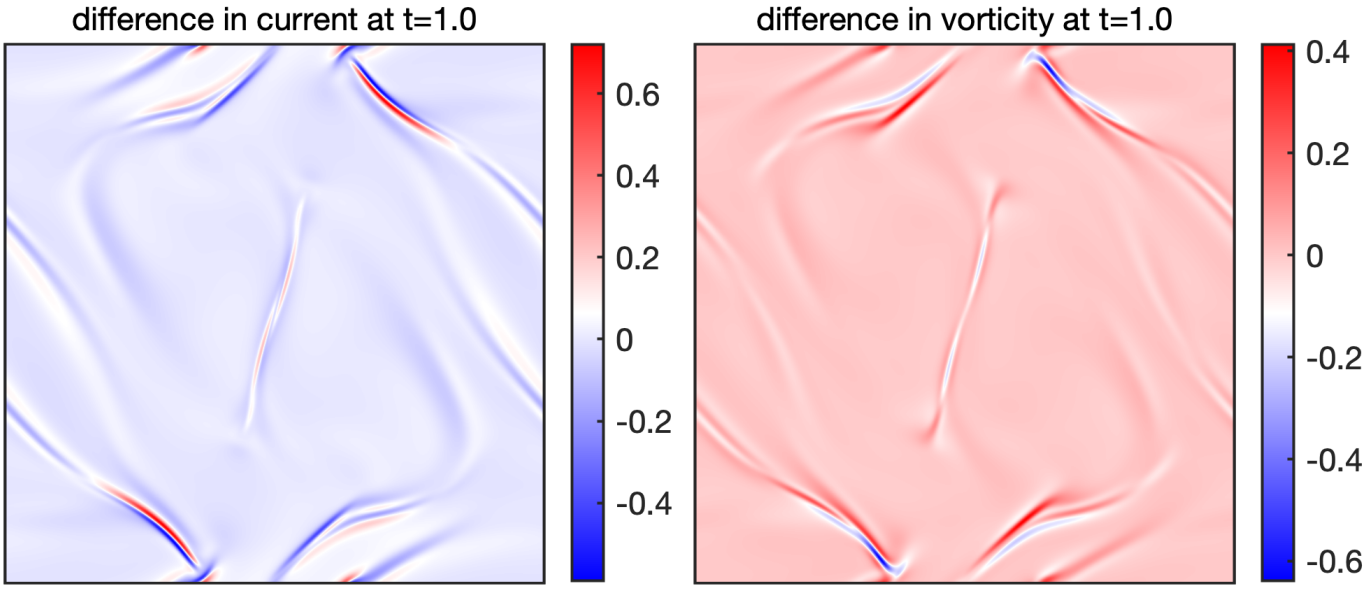

Fig. 8 Differences in the vorticity and current at t = 1.0 in the Orszag–Tang vortex simulated with the original scheme and the Lorentz force schemes on lattices with 4096 × 4096 points.

scheme [25]. The latter already includes a parabolic divergence cleaning term to diffuse $\nabla\cdot\mathbf{B}$, so the main improvement is the restoration of Galilean invariance, and a noticeable improvement in stability from using the Lorentz force scheme.

Acknowledgement

The computations employed the Advanced Research Computing facilities at the University of Oxford [73].

References

[1] Brackbill, J. U., and Barnes, D. C., "The effect of nonzero $\nabla\cdot\mathbf{B}$ on the numerical solution of the magnetohydrodynamic equations," *Journal of Computational Physics*, Vol. 35, No. 3, 1980, pp. 426–430. https://doi.org/10.1016/0021-9991(80)90079-0.

[2] Tóth, G., "The $\nabla\cdot\mathbf{B}=0$ constraint in shock-capturing magnetohydrodynamics codes," *Journal of Computational Physics*, Vol. 161, No. 2, 2000, pp. 605–652. https://doi.org/10.1006/jcph.2000.6519.

[3] Kemm, F., "On the origin of divergence errors in MHD simulations and consequences for numerical schemes," *Communications in Applied Mathematics and Computer Science*, Vol. 8, No. 1, 2013, pp. 1–38. https://doi.org/10.2140/camcos.2013.8.1.

[4] Boris, J. P., "Relativistic plasma simulation – optimization of a hybrid code," *Proceedings of the 4th Conference on Numerical Simulation of Plasmas*, edited by J. P. Boris and R. A. Shanny, Naval Research Laboratory, Washington, DC, 1972, pp. 3–67.

[5] Evans, C. R., and Hawley, J. F., "Simulation of magnetohydrodynamic flows – A constrained transport method," *Astrophysical Journal*, Vol. 332, Sep. 1988, pp. 659–677. https://doi.org/10.1086/166684.

[6] DeVore, C. R., "Flux-corrected transport techniques for multidimensional compressible magnetohydrodynamics," *Journal of Computational Physics*, Vol. 92, No. 1, 1991, pp. 142–160. https://doi.org/10.1016/0021-9991(91)90295-V.

[7] Hyman, J. M., and Shashkov, M., "Mimetic discretizations for Maxwell's equations," *Journal of Computational Physics*, Vol. 151, No. 2, 1999, pp. 881–909. https://doi.org/10.1006/jcph.1999.6225.

[8] Marder, B., "A method for incorporating Gauss' law into electromagnetic PIC codes," *Journal of Computational Physics*, Vol. 68, No. 1, 1987, pp. 48–55. https://doi.org/10.1016/0021-9991(87)90043-X.

[9] Assous, F., Degond, P., Heintze, E., Raviart, P. A., and Segre, J., "On a finite-element method for solving the three-dimensional Maxwell equations," *Journal of Computational Physics*, Vol. 109, No. 2, 1993, pp. 222–237. https://doi.org/10.1006/jcph.1993.1214.

[10] Munz, C.-D., Schneider, R., Sonnendrücker, E., and Voss, U., "Maxwell's equations when the charge conservation is not

satisfied," *Comptes Rendus de l'Academie des Sciences – Series I – Mathematics*, Vol. 328, No. 5, 1999, pp. 431–436. https://doi.org/10.1016/S0764-4442(99)80185-2.

[11] Kemm, F., Munz, C.-D., Schneider, R., and Sonnendrücker, E., "Divergence corrections in the numerical simulation of electromagnetic wave propagation," *Hyperbolic Problems: Theory, Numerics, Applications*, edited by H. Freistühler and G. Warnecke, Birkhäuser, Basel, 2001, pp. 603–612. https://doi.org/10.1007/978-3-0348-8372-6_14.

[12] Dedner, A., Kemm, F., Kroner, D., Munz, C. D., Schnitzer, T., and Wesenberg, M., "Hyperbolic divergence cleaning for the MHD equations," *Journal of Computational Physics*, Vol. 175, No. 2, 2002, pp. 645–673. https://doi.org/10.1006/jcph.2001.6961.

[13] Powell, K. G., "An approximate Riemann solver for magnetohydrodynamics (that works in more than one dimension)," ICASE Report No. 94-24, NASA Langley Research Center, Apr. 1994. Available from http://hdl.handle.net/2060/19940028527.

[14] Powell, K. G., Roe, P. L., Linde, T. J., Gombosi, T. I., and De Zeeuw, D. L., "A solution-adaptive upwind scheme for idea magnetohydrodynamics," *Journal of Computational Physics*, Vol. 154, No. 2, 1999, pp. 284–309. https://doi.org/10.1006/jcph.1999.6299.

[15] Tricco, T. S., and Price, D. J., "Constrained hyperbolic divergence cleaning for smoothed particle magnetohydrodynamics," *Journal of Computational Physics*, Vol. 231, No. 21, 2012, pp. 7214–7236. https://doi.org/10.1016/j.jcp.2012.06.039.

[16] Derigs, D., Winters, A. R., Gassner, G. J., Walch, S., and Bohm, M., "Ideal GLM-MHD: About the entropy consistent nine-wave magnetic field divergence diminishing ideal magnetohydrodynamics equations," *Journal of Computational Physics*, Vol. 364, July 2018, pp. 420–467. https://doi.org/10.1016/j.jcp.2018.03.002.

[17] Benzi, R., Succi, S., and Vergassola, M., "The lattice Boltzmann equation: theory and applications," *Physics Reports*, Vol. 222, No. 3, 1992, pp. 145–197. https://doi.org/10.1016/0370-1573(92)90090-M.

[18] Krüger, T., Kusumaatmaja, H., Kuzmin, A., Shardt, O., Silva, G., and Viggen, E. M., *The Lattice Boltzmann Method*, Springer, Cham, 2017. https://doi.org/10.1007/978-3-319-44649-3.

[19] Succi, S., *The Lattice Boltzmann Equation: For Complex States of Flowing Matter*, Oxford University Press, Oxford, 2018. https://doi.org/10.1093/oso/9780199592357.001.0001.

[20] Lallemand, P., Luo, L.-S., Krafczyk, M., and Yong, W.-A., "The lattice Boltzmann method for nearly incompressible flows," *Journal of Computational Physics*, Vol. 431, Apr. 2021, Paper 109713. https://doi.org/10.1016/j.jcp.2020.109713.

[21] Gatignol, R., *Théorie Cinétique des Gaz a Répartition Discrete de Vitesses*, Springer, Berlin, Heidelberg, 1975. https://doi.org/10.1007/3-540-07156-3.

[22] Cabannes, H., "The Discrete Boltzmann Equation (Theory and Application)," Lectures Notes, University of California, Berkeley, 1980. Available from http://henri.cabannes.free.fr/Cours_de_Berkeley.pdf.

[23] Chen, H., Matthaeus, W. H., and Klein, L. W., "An analytic theory and formulation of a local magnetohydrodynamic lattice gas model," *Physics of Fluids*, Vol. 31, No. 6, 1988, pp. 1439–1455. https://doi.org/10.1063/1.866735.

[24] Chen, S., Chen, H., Martínez, D. O., and Matthaeus, W. H., "Lattice Boltzmann model for simulation of magnetohydrodynamics," *Physical Review Letters*, Vol. 67, No. 27, 1991, pp. 3776–3779. https://doi.org/10.1103/PhysRevLett.67.3776.

[25] Dellar, P. J., "Lattice kinetic schemes for magnetohydrodynamics," *Journal of Computational Physics*, Vol. 179, No. 1, 2002, pp. 95–126. https://doi.org/10.1006/jcph.2002.7044.

[26] Dellar, P. J., "Moment equations for magnetohydrodynamics," *Journal of Statistical Mechanics*, Vol. 2009, June 2009, Paper P06003. https://doi.org/10.1088/1742-5468/2009/06/P06003.

[27] Dellar, P. J., "Lattice Boltzmann magnetohydrodynamics with current-dependent resistivity," *Journal of Computational Physics*, Vol. 237, Mar. 2013, pp. 115–131. https://doi.org/10.1016/j.jcp.2012.11.021.

[28] Breyiannis, G., and Valougeorgis, D., "Lattice kinetic simulations in three-dimensional magnetohydrodynamics," *Physical Review E*, Vol. 69, No. 6, 2004, Paper 065702. https://doi.org/10.1103/PhysRevE.69.065702.

[29] Vahala, G., Keating, B., Soe, M., Yepez, J., Vahala, L., Carter, J., and Ziegeler, S., "MHD turbulence studies using lattice Boltzmann algorithms," *Communications in Computational Physics*, Vol. 4, No. 3, 2008, pp. 624–646.

[30] Pattison, M., Premnath, K., Morley, N., and Abdou, M., "Progress in lattice Boltzmann methods for magnetohydrodynamic flows relevant to fusion applications," *Fusion Engineering Design*, Vol. 83, No. 4, 2008, pp. 557–572. https://doi.org/10.1016/j.fusengdes.2007.10.005.

[31] Li, J., Chua, K. T. E., Li, H., Nguyen, V.-T., Wise, D. J., Xu, G. X., Kang, C. W., and Chan, W. H. R., "On the consistency of three-dimensional magnetohydrodynamical lattice Boltzmann models," *Applied Mathematical Modelling*, Vol. 132, Aug. 2024, pp. 751–765. https://doi.org/doi:10.1016/j.apm.2024.04.028.

[32] Dellar, P. J., "Hyperbolic divergence cleaning in lattice Boltzmann magnetohydrodynamics," *Communications in Computational Physics*, Vol. 33, No. 1, 2023, pp. 245–272. https://doi.org/10.4208/cicp.OA-2022-0054.

[33] Baty, H., Drui, F., Helluy, P., Franck, E., Klingenberg, C., and Thanhäuser, L., "A robust and efficient solver based on kinetic schemes for magnetohydrodynamics (MHD) equations," *Applied Mathematics and Computation*, Vol. 440, Mar. 2023, Paper 127667. https://doi.org/10.1016/j.amc.2022.127667.

[34] Dellar, P. J., "A magic two-relaxation-time lattice Boltzmann algorithm for magnetohydrodynamics," *Discrete & Continuous Dynamical Systems, Series S*, 2023. https://doi.org/10.3934/dcdss.2023157, published online Sep. 2023.

[35] Jeffery, G. B., "The motion of ellipsoidal particles immersed in a viscous fluid," *Proceedings of the Royal Society of London, Series A*, Vol. 102, No. 715, 1922, pp. 161–179. https://doi.org/10.1098/rspa.1922.0078.

[36] Bretherton, F. P., "The motion of rigid particles in a shear flow at low Reynolds number," *Journal of Fluid Mechanics*, Vol. 14, No. 2, 1962, pp. 284–304. https://doi.org/10.1017/S002211206200124X.

[37] Junk, M., and Illner, R., "A new derivation of Jeffery's equation," *Journal of Mathematical Fluid Mechanics*, Vol. 9, No. 4, 2007, pp. 455–488. https://doi.org/10.1007/s00021-005-0208-0.

[38] Dellar, P. J., "Vector lattice Boltzmann equations: From magnetohydrodynamics to active matter," *Progress in Industrial Mathematics at ECMI 2021*, edited by M. Ehrhardt and M. Günther, Springer, Cham, 2022, pp. 407–416. https://doi.org/10.1007/978-3-031-11818-0_53.

[39] Landau, L. D., and Lifshitz, E. M., *Classical Theory of Fields*, 4th ed., Pergamon, Oxford, 1975. https://doi.org/10.1016/c2009-0-14608-1.

[40] Jackson, J. D., *Classical Electrodynamics*, 3rd ed., Wiley, New York, 1999. https://doi.org/10.1002/3527600434.eap109.

[41] Rindler, W., *Introduction to Special Relativity*, Oxford University Press, Oxford, 1982.

[42] Janhunen, P., "A positive conservative method for magnetohydrodynamics based on HLL and Roe methods," *Journal of Computational Physics*, Vol. 160, No. 2, 2000, pp. 649–661. https://doi.org/10.1006/jcph.2000.6479.

[43] Boillat, G., "Involutions des systémes conservatifs," *Comptes Rendus de l'Academie des Sciences – Series I – Mathematics*, Vol. 307, No. 17, 1988, pp. 891–894.

[44] Dafermos, C., "Hyperbolic conservation laws with involutions and contingent entropies," *Recent Advances in Nonlinear Partial Differential Equations and Applications*, edited by L. L. Bonilla, A. Carpio, J. M. Vega, and S. Venakides, American Mathematical Society, Providence, RI, 2007, pp. 193–217. https://doi.org/10.1090/psapm/065/2381880.

[45] Godunov, S. K., "Symmetric form of the magnetohydrodynamic equation," *Numerical Methods for Mechanics of Continuous Media*, Vol. 3, No. 1, 1972, pp. 26–34. In Russian.

[46] Majda, A., *Compressible Fluid Flow and Systems of Conservation Laws in Several Space Variables*, Springer, New York, 1984. https://doi.org/10.1007/978-1-4612-1116-7.

[47] Godlewski, E., and Raviart, P.-A., *Numerical Approximation of Hyperbolic Systems of Conservation Laws*, Springer, New York, 1996. https://doi.org/10.1007/978-1-4612-0713-9.

[48] Dellar, P. J., "Hamiltonian and symmetric hyperbolic structures of shallow water magnetohydrodynamics," *Physics of Plasmas*, Vol. 9, No. 4, 2002, pp. 1130–1136. https://doi.org/10.1063/1.1463415.

[49] Morrison, P. J., "Poisson brackets for fluids and plasmas," *Mathematical Methods in Hydrodynamics and Integrability of Dynamical Systems*, edited by M. Tabor and Y. M. Treve, American Institute of Physics, New York, 1982, pp. 13–46. https://doi.org/10.1063/1.33633.

[50] Morrison, P. J., "Hamiltonian description of the ideal fluid," *Reviews of Modern Physics*, Vol. 70, No. 2, 1998, pp. 467–521. https://doi.org/10.1103/RevModPhys.70.467.

[51] Morrison, P. J., and Greene, J. M., "Noncanonical Hamiltonian density formulation of hydrodynamics and ideal magnetohydrodynamics," *Physical Review Letters*, Vol. 45, No. 10, 1980, pp. 790–794. https://doi.org/10.1103/PhysRevLett.45.790, erratum: Vol. 48, No. 8, 1982, p. 569. https://doi.org/10.1103/PhysRevLett.48.569.

[52] Holm, D. D., and Kupershmidt, B. A., "Hamiltonian theory of relativistic magnetohydrodynamics with anisotropic pressure," *Physics of Fluids*, Vol. 29, No. 11, 1986, pp. 3889–3891. https://doi.org/10.1063/1.865774.

[53] Dellar, P. J., "A note on magnetic monopoles and the one dimensional MHD Riemann problem," *Journal of Computational Physics*, Vol. 172, No. 1, 2001, pp. 392–398. https://doi.org/10.1006/jcph.2001.6815.

[54] Cercignani, C., *The Boltzmann Equation and its Applications*, Springer, New York, 1988.

[55] Qian, Y. H., d'Humières, D., and Lallemand, P., "Lattice BGK models for the Navier–Stokes equation," *Europhysics Letters*, Vol. 17, No. 6, 1992, pp. 479–484. https://doi.org/10.1209/0295-5075/17/6/001.

[56] He, X., and Luo, L.-S., "Theory of the lattice Boltzmann method: From the Boltzmann equation to the lattice Boltzmann equation," *Physical Review E*, Vol. 56, No. 6, 1997, pp. 6811–6817. https://doi.org/10.1103/PhysRevE.56.6811.

[57] Luo, L.-S., "Unified theory of lattice Boltzmann models for nonideal gases," *Physical Review Letters*, Vol. 81, No. 8, 1998, pp. 1618–1621. https://doi.org/10.1103/PhysRevLett.81.1618.

[58] Qian, Y. H., and Orszag, S. A., "Lattice BGK models for the Navier–Stokes equation: Nonlinear deviation in compressible regimes," *Europhysics Letters*, Vol. 21, No. 3, 1993, pp. 255–259. https://doi.org/10.1209/0295-5075/21/3/001.

[59] Strang, G., "On the construction and comparison of difference schemes," *SIAM Journal of Numerical Analysis*, Vol. 5, No. 3, 1968, pp. 506–517. https://doi.org/10.1137/0705041.

[60] Dellar, P. J., "An interpretation and derivation of the lattice Boltzmann method using Strang splitting," *Computers and Mathematics with Applications*, Vol. 65, No. 2, 2013, pp. 129–141. https://doi.org/10.1016/j.camwa.2011.08.047.

[61] Crank, J., and Nicolson, P., "A practical method for numerical evaluation of solutions of partial differential equations of the heat-conduction type," *Mathematical Proceedings of the Cambridge Philosophical Society*, Vol. 43, No. 1, 1947, pp. 50–67. https://doi.org/10.1017/S0305004100023197.

[62] Bhatnagar, P. L., Gross, E. P., and Krook, M., "A model for collision processes in gases. I. Small amplitude processes in charged and neutral one-component system," *Physical Review*, Vol. 94, No. 3, 1954, pp. 511–525. https://doi.org/10.1103/PhysRev.94.511.

[63] Hénon, M., "Viscosity of a lattice gas," *Complex Systems*, Vol. 1, No. 4, 1987, pp. 763–789.

[64] Dellar, P. J., "Lattice Boltzmann formulation for linear viscoelastic fluids using an abstract second stress," *SIAM Journal of Scientific Computing*, Vol. 36, No. 6, 2014, pp. A2507–A2532. https://doi.org/10.1137/130940372.

[65] He, X., Chen, S., and Doolen, G. D., "A novel thermal model of the lattice Boltzmann method in incompressible limit," *Journal of Computational Physics*, Vol. 146, No. 1, 1998, pp. 282–300. https://doi.org/10.1006/jcph.1998.6057.

[66] Brownlee, R. A., Gorban, A. N., and Levesley, J., "Stability and stabilization of the lattice Boltzmann method," *Physical Review E*, Vol. 75, No. 3, 2007, Paper 036711. https://doi.org/10.1103/PhysRevE.75.036711.

[67] Kupershtokh, A. L., "New method of incorporating a body force term into the lattice Boltzmann equation," *Proc. 5th International EHD Workshop, August 30-31, 2004, Poitiers, France*, 2004, pp. 241–246. Available from http://ancient.hydro.nsc.ru/sk/EHD-2004/FR2004-LBE.pdf.

[68] Kupershtokh, A. L., "Criterion of numerical instability of liquid state in LBE simulations," *Computers and Mathematics with Applications*, Vol. 59, No. 7, 2010, pp. 2236–2245. https://doi.org/10.1016/j.camwa.2009.08.058.

[69] Dellar, P. J., "Incompressible limits of lattice Boltzmann equations using multiple relaxation times," *Journal of Computational Physics*, Vol. 190, No. 2, 2003, pp. 351–370. https://doi.org/doi:10.1016/S0021-9991(03)00279-1.

[70] Wagner, A. J., "The origin of spurious velocities in lattice Boltzmann," *International Journal of Modern Physics B*, Vol. 17, No. 1 & 2, 2003, pp. 193–196. https://doi.org/10.1142/S0217979203017448.

[71] Connington, K., and Lee, T., "A review of spurious currents in the lattice Boltzmann method for multiphase flows," *Journal of Mechanical Science and Technology*, Vol. 26, Dec. 2012, pp. 3857–3863. https://doi.org/10.1007/s12206-012-1011-5.

[72] Orszag, S. A., and Tang, C.-M., "Small-scale structure of two-dimensional magnetohydrodynamic turbulence," *Journal of Fluid Mechanics*, Vol. 90, No. 1, 1979, pp. 129–143. https://doi.org/10.1017/S002211207900210X.

[73] Richards, A., "University of Oxford Advanced Research Computing," Technical Note, 2015. Available from https://doi.org/10.5281/zenodo.22558.